2019

Measurement of Changes in Heme Ruffling Caused by the Staphylococcus aureus Heme-Degrading Enzyme, IsdG

Amanda Rose Cornetta

Measurement of Changes in Heme Ruffling Caused by the *Staphylococcus aureus* Heme-Degrading Enzyme, IsdG

A Thesis Presented

by

Amanda Cornetta

to

The Faculty of the College of Arts & Sciences

of

The University of Vermont

In Partial Fulfillment of the Requirements
of the University of Vermont Honors College

May 2019

Defense Date: April 25, 2019

Thesis Defense Committee:
Matthew D. Liptak, Ph.D., Advisor
Jay Silveira, Ph.D., Chair
Matthias Brewer, Ph.D.

ABSTRACT

Staphylococcus aureus is one of the most common causes of infection and has been rapidly developing drug resistance, making the discovery of a new drug target imperative. This project analyzed the interaction between heme and IsdG, a heme degrading enzyme involved in the spread of *S. aureus*, to gain further insight into the mechanism of heme degradation. Iron serves as an essential nutrient for *S. aureus*, and IsdG is the primary enzyme involved in iron acquisition from heme. IsdG has a catalytic pocket that contains tryptophan at residue 67 that is expected to be involved in heme ruffling. The W67F variant of IsdG formed with site-directed mutagenesis was expected to ruffle and degrade heme to a lesser extent being that Trp is replaced with a less bulky amino acid, Phenylalanine (Phe, F). The variant was characterized using Electronic Absorption (Abs), Ultraviolet Circular Dichroism (UV CD), and Magnetic Circular Dichroism (MCD) spectroscopies to analyze changes to the geometric and electronic structure resulting from the substitution. The CD spectra confirmed similar geometric structures of W67F and wild-type (WT) IsdG. The activity of W67F differed from that of WT IsdG, indicating that Trp67 is involved in the enzyme's activity and promotes IsdG turnover. The Abs spectra showed a blue-shift in the Q and Soret bands of W67F IsdG indicating reduced heme ruffling and that Trp67 was involved in heme ruffling. The increased intensity of the negative-component of the Soret band in the MCD spectrum of W67F IsdG was indicative of a ^2E_g electronic ground state, consistent with reduced heme ruffling. Being that Trp67 is an active site residue specific to the IsdG family of non-canonical heme oxygenases (HOs), this information regarding the influence of Trp67 on heme ruffling and IsdG activity is crucial to the development of a selective inhibitor of IsdG in the presence of canonical HOs.

ABBREVIATIONS

Abs	Electronic absorption
CD	Circular Dichroism
DTT	Dithiothreitol
EDTA	Ethylenediaminetetraacetic acid
FPLC	Fast protein liquid chromatography
HO	Heme oxygenase
IPTG	Isopropyl β-D-1-thiogalactopyranoside
Isd	Iron-regulated surface determinant
IsdG–heme	Heme-bound IsdG
IsdG–heme–CN	Cyanide-inhibited IsdG
KPi	Potassium phosphate
MCD	Magnetic circular dichroism
MRSA	Methicillin-resistant *Staphylococcus aureus*
NaPi	Sodium phosphate
nCHO	Non-canonical heme oxygenase
PMSF	Phenylmethanesulfonylfluoride fluoride
SOC	Spin orbit coupling
TEV	Tobacco etch virus
UV-CD	Ultraviolet CD
VTVH	Variable-temperature, variable-field
WT	Wild-type

INTRODUCTION

Staphylococcus aureus is one of the leading causes of healthcare-associated infection in the United States (US). It is highly communicable and especially life-threatening to those with compromised immune systems. Furthermore, drug-resistant strains of this bacterium exist, such as methicillin-resistant *S. aureus* (MRSA). MRSA has been achieving stronger resistance to commonly used antibiotics and is one of the leading causes of mortality in the US.[1] According to the *Centers for Disease Control and Prevention,* there were over 80,000 severe cases of healthcare-associated MRSA that resulted in over 11,000 deaths in the US in 2011.[2] Additionally, the rates of community-associated MRSA, infection in the general population that was not contracted from being in a healthcare setting, have increased rapidly over the past decade.[2] With this being said, understanding the mechanism by which *S. aureus* infects the human host provides information crucial to the design of a new drug to target and prevent this process. Designing a drug to combat *S. aureus* requires the identification of a reaction that is unique to the bacterium's metabolism as a drug target.

Iron is an essential nutrient used by *S. aureus* to power its pathogenesis throughout the eukaryotic host. The iron-containing porphyrin compound heme is the bacteria's primary source of iron. Heme is found within various biological molecules in the eukaryotic host including hemoglobin, in which it is used to bind and transport oxygen to tissues throughout the host.[3] IsdG has been discovered to be the primary enzyme involved in the iron acquisition pathway from heme by *S. aureus*.[4] IsdG belongs to a family of nine iron-regulated surface determinant (Isd) proteins that are also involved in the iron acquisition and heme degradation pathway.[5] A model has been proposed regarding the role each enzyme in the Isd family plays in the iron acquisition pathway by *S. aureus*. It is hypothesized that *S. aureus* first produces toxins such as hemolysins that lyse

red blood cells, releasing hemoglobin. IsdH and IsdB, located along the cell wall, bind free hemoglobin and remove heme for transfer to IsdA and IsdC (Figure 1). Heme is transported through the cell wall into the cytoplasm using the membrane transporter composed of IsdDEF. Within the cytoplasm, IsdG and IsdI, a paralog of IsdG that has a similar structure and reaction products, degrade heme and liberate iron.[6] Being that IsdG is the main enzyme involved in iron acquisition, the inhibition of this enzyme would starve *S. aureus* of the iron that is essential to the bacteria's pathogenesis, making IsdG a potentially promising drug target.[4]

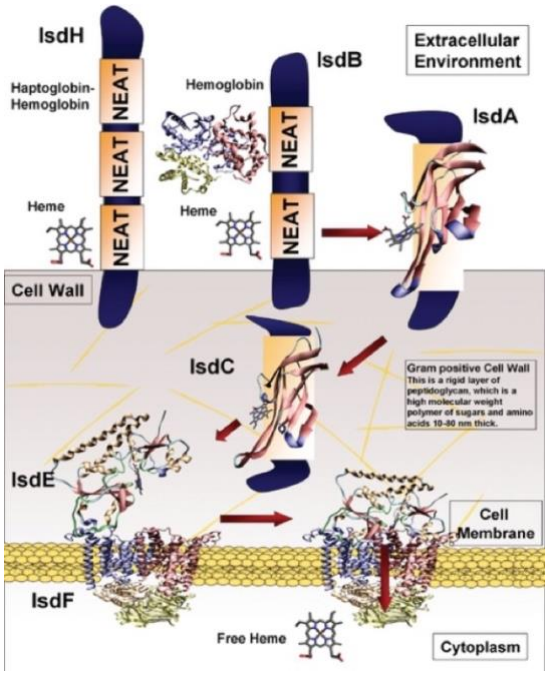

Figure 1. Proposed Isd heme-scavenging pathway used by *S. aureus*.[7] The proposed pathway involves the binding of hemoglobin to IsdH and IsdB, which transfer heme to IsdA (PDB ID: 2ITF), IsdC (PDB ID: 2O6P), and IsdE (PDB ID: 2Q8Q). The transporter protein complex IsdDEF transports heme across the cell membrane into the cytoplasm where IsdG is located. Figure adapted from Ref. #7.

The eukaryotic host also contains canonical HOs that have similar enzymatic functions to the non-canonical HO (nCHO) IsdG and also degrade heme. To develop a new drug target that selectively inhibits IsdG in the presence of canonical HOs, the differences between IsdG and

canonical HOs must be considered. Both canonical HOs and IsdG utilize the same substrates, heme and molecular oxygen; however, they convert these reactants into different products through different reaction mechanisms. Canonical HOs catalyze the oxidative degradation of heme into biliverdin, a dioxygenated tetrapyrrole, carbon monoxide and free iron (Figure 2). The proposed mechanism of heme degradation by canonical HOs begins with the reduction of Fe(III) to Fe(II) by NADPH-cytochrome P450 reductase and the binding of a peroxo ligand. The resultant intermediate is further reduced by the reductase into a hydroperoxide heme intermediate. The compound self-hydroxylates at the α-*meso* carbon of the porphyrin ring, forming α-meso-hydroxyheme, which undergoes additional oxidoreductive steps to form biliverdin (Figure 2). [8]

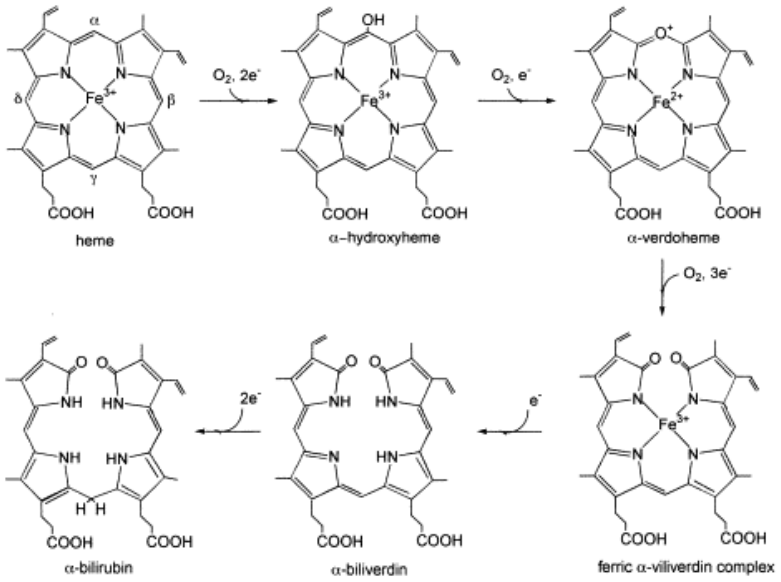

Figure 2. Pathway of heme degradation by canonical HOs.[8] The transformation of heme to biliverdin is catalyzed by HO and the reaction of biliverdin into bilirubin is catalyzed by biliverdin reductase. Figure adapted from Ref. #8.

On the other hand, nCHOs such IsdG produce staphylobilins, trioxygenated tetrapyrroles, formaldehyde and free iron (Figure 3). Previous studies have determined that heme degradation by IsdG yields staphylobilins through ferric-peroxoheme and meso-hydroxyheme intermediates.

However, the mechanism for the conversion between these intermediates is not well understood.[9] It has been determined that the reductase catalyzing the reactions is IruO.[10] During this reaction the porphyrin complex is hydroxylated at the β- or δ-*meso* carbon, rather than at the α-*meso* carbon, as is the case with canonical HOs.[11] This results in the formation of 5-oxo-δ-bilirubin or 15-oxo-β-bilirubin, also known as staphylobilins, and formaldehyde rather than CO.[12] The lack of CO production indicates that the IsdG reaction does not involve verdoheme, a key intermediate in the canonical HO heme degradation reaction that results in the production of CO. Further insight into the mechanism of IsdG is crucial to the development of a potential therapeutic drug target that is specific to IsdG and not canonical HOs.

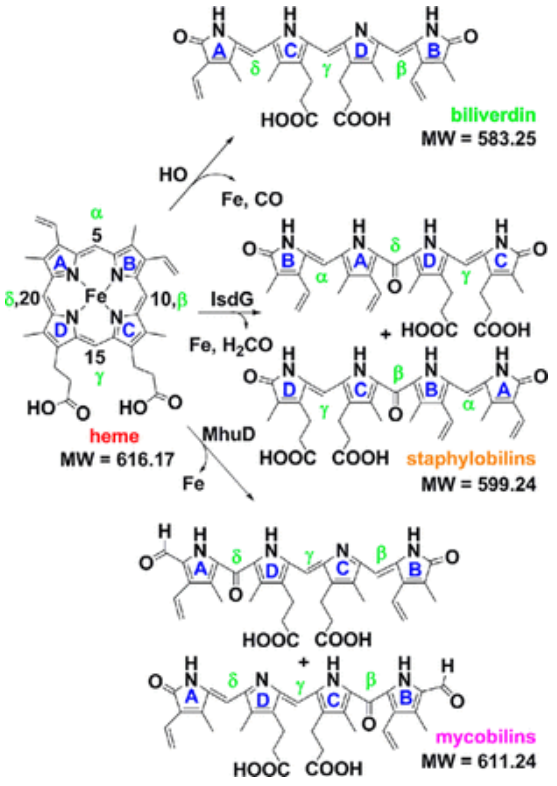

Figure 3. Reaction products from heme degradation by HO, IsdG and MhuD.[11] Each reaction pathway results in the formation of different products. Figure adapted from Ref #11.

Moreover, the structure of IsdG differs from that of canonical HOs. IsdG consists of homodimeric β-barrel structures with two active sites that contrasts with the α-helical structure of canonical HOs.[13] Also, various active site residues of IsdG were confirmed to be involved in the heme degradation reaction by studying the effect that a substitution to each residue had on the heme degradation rate. These included Asn7, Met38, Trp67 and His77. Asn7, Trp67, and His77 were substituted for Alanine, which completely eliminated IsdG activity in these variants. Alanine substitution of Met38 resulted in a slight reduction of IsdG activity and shifted the Soret band absorbance from about 410 to 430 nm as a result of changes to the interaction between IsdG and heme resulting from the substitution.[13] Substitutions of residues predicted to be outside of the catalytic pocket of IsdG were found to have no significant effect on IsdG activity, as was expected being that such residues do not form as strong of interactions with the heme substrate as the active site residues.[13] Additionally, at least two of these second-sphere residues are known to be unique to the active site of IsdG and not found in human HOs, including Asn7 and Trp67.[13] Similar to the differences in the reaction mechanisms of IsdG and canonical HOs, their structural differences also serve as useful information for the development of a drug target specific to IsdG.

The structure of heme-bound IsdG (IsdG–heme) has been determined from a previous study generated the X-ray crystal structure of N7A IsdG–heme, the only crystal structure available for heme-bound IsdG.[14] This structure illustrated that heme forms hydrophobic interactions with various residues including Leu9, Phe23, Phe64, Trp67, Leu68 and Val80. The side chain of Trp67 forms a steric contact with the β-*meso* carbon in heme (Figure 4C). This interaction resulted in greater distortion or ruffling of the planar porphyrin ring of 2.0 Å than observed for other heme-binding proteins, including HOs which distort it by less than 0.5 Å.[14] The nonplanarity of heme when bound to IsdG suggests that the mechanism of heme degradation by IsdG is different from

that of canonical HOs. Moreover, the extent of heme ruffling has been seen to be related to the activity of IsdG. The W67A variant of IsdG was found to have reduced activity being that the substitution of Trp with Alanine eliminated the steric contact that forms between Trp and the β-*meso* carbon in heme that plays a role in distorting heme.[14] More specifically, heme ruffling has been determined to enhance the reactivity of the peroxoheme intermediate by orienting the β- or δ-*meso* carbons toward the oxygen species.[14] As a result of this, heme ruffling promotes the formation of aldehyde by IsdG, rather than CO produced by canonical HOs.[14] It has also been proposed that the extent of heme ruffling alters the electronic configuration of the intermediate species.[15] Overall, the nonplanarity of the heme when bound to IsdG is one of the most unique features about the enzyme that distinguishes it from canonical HOs.

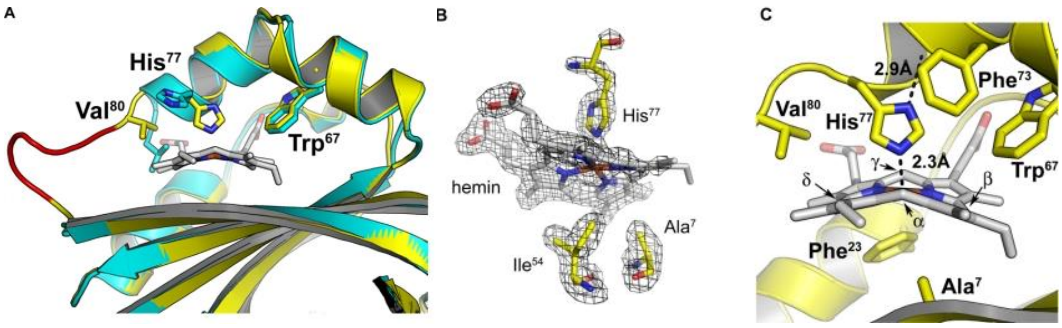

Figure 4. IsdG–heme structure.[14] A) Apo-IsdG (cyan) superimposed over IsdG–heme (yellow), B) IsdG active site viewed from the distal side, C) IsdG–heme active site with the residues that interact with heme. Figure adapted from Ref #14.

This study investigates the role of the active site residue, Trp67, which has been predicted to be involved in binding and degrading heme. Although Trp67 is known to be required for IsdG activity, it's specific role in the process is still being investigated. Trp67 has been found to form non-bonding interactions with the His–heme–O_2 moiety. It has been hypothesized that its role may include positioning heme with respect to the other residues in the active site and to stabilize the intermediate species formed during heme oxygenation, directly contributing to the ruffling of the

porphyrin ring of heme.[13] In this study, Trp67 was mutated into Alanine (Ala, A) and Phenylalanine (Phe, F), amino acids with smaller structures. The substitution of Trp to Phe was done in a previous study to the analogous Trp residue in IsdI. This substitution in IsdI resulted in reduced heme ruffling and enzymatic activity.[16] Therefore, W67F IsdG was also expected to result in reduced heme ruffling and enzymatic activity compared to that of WT IsdG. The effects of the W67A and W67F substitutions on the structure and enzymatic activity of IsdG were analyzed using ultraviolent circular dichroism (UV CD), electronic absorption (Abs), and magnetic CD (MCD) spectroscopies.

UV CD spectroscopy was used to visualize changes to the secondary structure of IsdG that resulted from the substitution of the active site residue. This provided information to assess whether any enzyme activity changes could be attributed to protein secondary structure changes. This technique involves shining left and right circular polarized light on a sample and a detector that determines the degree to which an optically active sample rotates the plane of polarized light. The specific CD peaks produced by the interaction of the circular polarized light with the sample in each spectrum correlate to the proportion of α-helices and β-sheets in the protein. A ratio of the two elements can be calculated from the data and used to quantify the changes in the secondary structure.[17] Further spectroscopic analyses were carried out on variants that had significantly similar proportions of these secondary structure elements.

Abs spectroscopy was used to compare the activity of WT and W67F IsdG–heme to determine whether the substitution reduced enzymatic activity as hypothesized. Abs spectra of heme-binding proteins contain a Soret peak that results from intraligand $\pi \rightarrow \pi^*$ transitions. The presence of heme bound in a protein's active site alters the location and shape of the Soret. Therefore, the changes in the Abs spectrum of the Soret band observed over time provide insight

into the rate of heme degradation by an enzyme in the presence of a reductant, such as ascorbate which is used in this study. Additionally, Abs spectroscopy was used to assess the amount of heme ruffling exerted by W67F IsdG. The amount of distortion of the porphyrin complex was determined using the PBE/TZVP TDDFT-predicted Abs spectra from a previous study involving a heme-bound nCHO, MhuD (Figure 5). The figure illustrates the dependence of the Q and Soret band energies on heme ruffling, which appear to red-shift with increased porphyrin ruffling greater than 1.0 Å.[18]

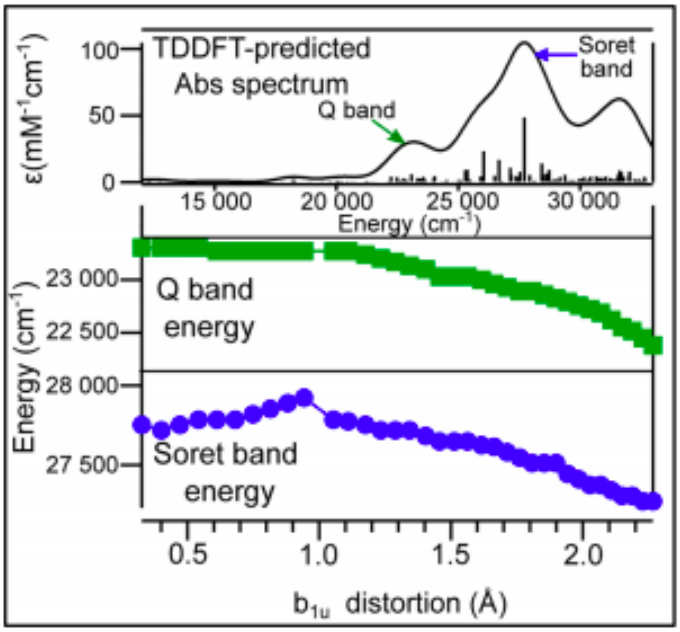

Figure 5. PBE/TZVP TDDFT-predicted Abs spectra from the X-ray crystal structure of WT MhuD–heme–CN (PDB ID 4NL5).[18] The model illustrates the relationship between the energy of the Q and Soret bands and the amount of heme ruffling in terms of b_{1u} out-of-plane distortion. Figure adapted from Ref #18.

Lastly, MCD spectroscopy was used to gain further information regarding electronic structures of WT and W67F IsdG. This technique involves the differential absorption of circularly polarized light in the presence of a magnetic field. The magnetic field creates a difference in the energy of electronic transitions in degenerate states, resulting in different types

of peaks that are labeled *A*, *B*, and *C* terms. The *C* term is a temperature-dependent absorption-shaped peak that arises from the splitting of a degenerate ground state in low temperature MCD spectroscopy. The *A* and *B* terms are temperature-independent peaks that are derivative and absorption-shaped, respectively. These terms contribute very little to the peaks seen at low temperatures being that they are temperature independent. Obtaining MCD data at cryogenic temperatures is useful in determining the ground state electron configuration.[19] Therefore, the MCD spectra of W67F and WT IsdG were compared to determine the electronic configuration of the Fe(III) in heme. For Abs and MCD spectroscopic analysis, cyanide was added and served as an analogue for the peroxo ligand that is normally involved in the heme degradation mechanism. CN, a π-acceptor ligand, promoted the formation of a low-spin Fe(III) complex.

METHODS

Protein Expression & Purification

The materials used in this work were purchased from Fisher Scientific and were not further purified, unless otherwise specified.

Expression of IsdG. Short-linker WT was cloned into a pET15b (Amp^r, Novagen) plasmid as previously described for long-linker WT IsdG (IBC protocol #: 12-017).[4, 6, 17] S219V tobacco etch virus (TEV) protease was cloned into a pRK793 (Amp^r) plasmid and expressed as previously described.[17, 20] The W67A and W67F substitutions were introduced into the *isdG* gene encoded within the pET15b plasmid through site-directed mutagenesis with the QuikChange Lightning site-directed mutagenesis kit (Agilent), as described for N7A IsdG.[17] A short-linker construct was used in the preparation of WT and W67F IsdG, which lacked the 12 amino acid N-terminal linker between the TEV protease cleavage site and the start of the *isdG* gene, rather than the long-linker construct used for W67A and in previous IsdG studies.[4, 6, 17] The DNA primers used to introduce the W67A and W67F substitutions were designed according to the guidelines in the kit and were purchased from the Midland Certified Reagent Company. The DNA was extracted using the QIAprep Spin Miniprep Kit (Qiagen). DNA sequencing at the University of Vermont Cancer Center DNA Analysis facility confirmed the WT sequence, the introduction of the substitutions and the deletion of the 12 amino acid linker. The pET15b plasmids encoding WT, W67A and W67F IsdG were then transformed into *Escherichia coli* BL21-GOLD (DE3) cells (Stratagene) and expressed as described for long-linker WT IsdG.[6] The cells were grown at 37 °C while shaken at 425 rpm using a Thermo Scientific MaxQ 5000 floor-model shaker for three hours. Upon reaching mid-log phase, an OD_{600} of 0.8, the cells were induced with 1.0 mM isopropyl β-D-1-thiogalactopyranoside (IPTG). Cell growth continued for four hours at 37 °C, and then the cells

harvested by centrifugation at 4 °C, 10,000 x *g* for 10 min using a Thermo Scientific Sorvall Legend XT centrifuge with a FiberLite F14-6x250 LE rotor. The resultant cell pellets were stored at -20 °C.

Purification of IsdG. The purification of WT and W67F IsdG followed the procedure used for long-linker IsdG with minor changes.[6] Each cell pellet was re-suspended in 25 mL of 50 mM Tris pH 7.4, 150 mM NaCl, 5 mM phenylmethanesulfonylfluoride fluoride (PMSF, Pierce) and 25 units of DNase1 (Pierce). Cells were lysed enzymatically through incubation with 0.1 mg/mL of lysozyme for 1 hr at room temperature. The lysate was centrifuged at 15,000 x *g*, 4 °C for 1 hr and the resulting supernatant was filtered through a 0.45 μm membrane using a desktop vacuum filter (Millipore). The filtered lysate were loaded onto a nickel-charged HiTrap Chelating HP column (GE Healthcare) that was equilibrated with 50 mM Tris pH 7.4, 150 mM NaCl using an Äkta Pure fast protein liquid chromatography (FPLC) system (GE Healthcare). The column was washed with a linear gradient of imidazole from 0 to 80 mM, before the IsdG variant was eluted with 250 mM imidazole. A similar procedure was used to purify the TEV cell pellet.[17, 20]

The N-terminal His_6-tag was removed using a procedure described for IsdI, another iron-regulated surface determinant enzyme.[4, 18] Purified S219V TEV protease was added to each of the purified His_6-tagged IsdG samples to form a solution of 10% TEV protease (*v*/v), 1 mM dithiothreitol (DTT), a reducing agent, and 0.5 mM ethylenediaminetetraacetic acid (EDTA), a chelating agent. The solution was concentrated and dialyzed against 1 L of 50 mM sodium phosphate (NaPi) pH 7.4, 300 mM NaCl for 3 hrs at 4 °C, and then again against 1 L of 50 mM Tris pH 7.4, 150 mM NaCl overnight at 4 °C. To remove the N-terminal His_6-tag, each protein solution was loaded onto a HisPur Ni-NTA column equilibrated and washed with 50 mM Tris pH 7.4, 150 mM NaCl, 20 mM imidazole. The untagged IsdG protein eventually eluted while the

S219V TEV protease remained adsorbed to the column. SDS-PAGE confirmed that the flow-through consisted of untagged IsdG samples each with > 90% purity (Figure 6).

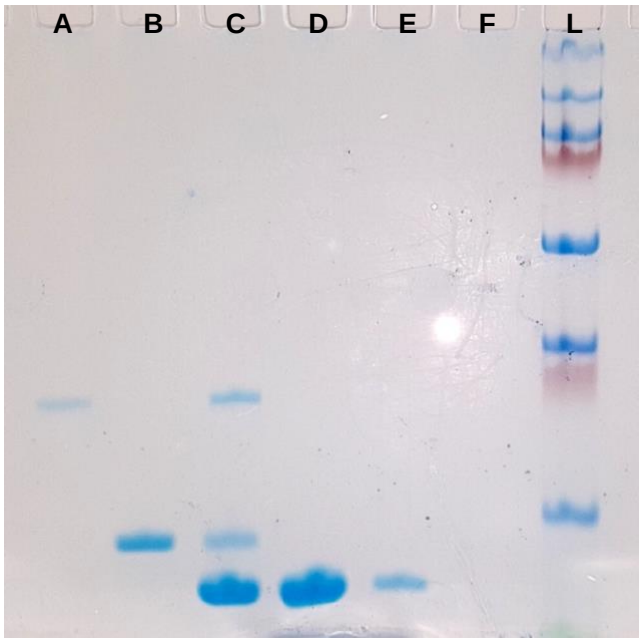

Figure 6. SDS-PAGE gel of W67F IsdG Purification. (A) Pure TEV Protease, (B) Uncleaved W67F IsdG, (C) Cleavage reaction, (D) Cleaved purified W67F IsdG at 12.6 kDa, (E) 1/10 dilution of cleaved W67F IsdG, (F) 1/100 dilution of cleaved W67F IsdG, (L) PageRuler Plus prestained protein ladder.

Substrate Binding

IsdG–Heme Sample Preparation. The purified untagged WT, W67A and W67F IsdG samples were combined with heme as outlined in the literature for other heme-bound HO complexes.[9] A 500 μM hemin chloride solution was prepared by first dissolving 3.3 mg of hemin chloride in 200 μL of 1.0 M NaOH, and then diluting the solution to a total volume of 10 mL with 50 mM Tris pH 7.4, 150 mM NaCl. The solution was back-titrated to a pH of 7.4 with 150 μL of 1.0 M HCl. The IsdG proteins were each combined with the hemin solution in a 1:1 molar ratio and then incubated at 4 °C for 1 hr. After, each IsdG–heme solution was exchanged into 10 mM

potassium phosphate (KPi) pH 7.4 using a PD-10 desalting column (GE Healthcare), removing any excess hemin in solution.

IsdG–Heme–CN Sample Preparation. To prepare cyanide-inhibited IsdG (IsdG–heme–CN) samples, a crystal of KCN was added to a solution of 500 μM hemin chloride in 50 mM Tris pH 7.4, 150 mM NaCl, prepared as described above, in a fume hood. The heme/CN solution and IsdG samples were combined in a 0.5:1 molar ratio and incubated at 4 °C for 1 hr. The resultant IsdG–heme–CN samples were exchanged into 10 mM KPi pH 7.4 using a PD-10 desalting column.

Spectroscopic Characterization

CD Spectroscopy. CD spectroscopy was used to compare the secondary structures of apo and holo forms of W67A and W67F IsdG to that of WT IsdG. Both apo and holo forms of WT, W67A and W67F IsdG were exchanged into 10 mM KPi pH 7.4 using PD-10 desalting columns and were loaded into a quartz cuvette of a 2 mm path length (Starna). Room temperature CD spectra were acquired from 260 to 185 nm with a scan speed of 20 nm/min, bandwidth of 1.0 nm, digital integration time of 8 s, and data pitch of 0.5 nm using a Jasco J-1700 Circular Dichroism Spectrophotometer.

The spectra were analyzed using the Dicroweb program CDSSTR to determine the proportions of the secondary structures in each IsdG variant. This program calculated the proportions of α-helices and β-sheets which were compared between the heme and apo forms of W67F versus WT IsdG. Root-mean-square-deviation (RMSD) error values calculated within a previous study were used to estimate the systemic error for the UV CD analysis.[21] No further spectroscopic characterization was used to analyze the W67A IsdG variant after UV CD analysis.

Abs Spectroscopy. The molar extinction coefficient for each sample was determined using the pyridine hemochrome assay, a method commonly used for heme-bound proteins in the literature.[22] The extinction coefficients calculated from the assays include the following: ε_{565} = 173.07 $mM^{-1}cm^{-1}$ for W67F IsdG–heme, ε_{418} = 133.67 $mM^{-1}cm^{-1}$ for W67F IsdG–heme–CN, and $\varepsilon_{420.5}$ = 94.9 $mM^{-1}cm^{-1}$ for WT IsdG–heme–CN.

Room temperature Abs spectra were collected for the W67F and WT IsdG–heme–CN samples in 50 mM Tris pH 7.4, 150 mM NaCl. Porphyrins, such as heme, have two intense bands, named the Q and Soret band, in the 400-600 nm region of the spectra that are commonly noted in the literature. The differences in energies of these peaks were used to quantify the difference in the amount of heme ruffling between W67F and WT IsdG–heme–CN using the QM/MM model described in a previous study.[18] The Abs spectra were collected on a Cary 100 Bio spectrophotometer from 700 to 300 nm with a scan rate of 600 nm/min, bandwidth of 2 nm, digital integration time of 0.1 s, and data interval of 1.0 nm.

MCD Spectroscopy. MCD spectroscopy was used to compare the electronic structures of W67F and WT IsdG–heme–CN. Samples of 10 μM and 100 μM W67F IsdG–heme–CN were prepared to visualize the Soret and Q bands, respectively. Each protein was first exchanged into 125 mM KPi pH 7.4 using a PD-10 desalting column and concentrated. The protein solutions were combined with glycerol, to protect the sample from damage at cryogenic temperatures, and CN^- to yield a final solution of 50 mM KPi pH 7.4, excess CN^-, and 60% (*v*/v) glycerol. The samples were loaded into a custom-built oxygen-free copper/quartz cuvette of a 2 mm path length and flash frozen in liquid nitrogen. The samples were stored in liquid nitrogen within a Bio-Cane™ canister. MCD spectra and VTVH MCD saturation magnetization curves were acquired on a setup of a Jasco J-815 spectropolarimeter and an Oxford SM4000-8T Spectromag controlled by a Mercury

iTC temperature controller and Mercury iPS power supply. Cryogenic temperature spectral data were acquired between 800 and 300 nm for the 10 μM sample and between 800 and 475 nm for the 100 μM sample. The data were acquired as a function of magnetic field strength at 2, 5, 10, and 20 K with a scanning speed of 200 nm/min, bandwidth of 1 nm, digital integration time of 0.25 s, and a data pitch of 0.5 nm.

Igor Pro was used to analyze all CD and MCD data collected. The data in the spectra were converted to Δε units using the following calculation: $\Delta\varepsilon = \frac{mdeg}{3298*c*\ell}$, in which "c" is the concentration of the protein in the sample and "ℓ" is the path length of the cuvette. The path length of the cuvette used was 0.2 cm for CD spectroscopy and 0.3 cm for MCD spectroscopy. The natural CD spectrum contribution was removed from all MCD data in this work by dividing by the difference between the positive and negative magnetic field data by two.

Activity Assays

Activity Assay Preparation. The activities of WT and W67F IsdG–heme were determined by reacting each protein with heme as has been done in previous studies.[6, 18] The activities were measured in the presence of catalase and both in the absence and presence of superoxide dismutase (SOD). In the absence of SOD, the reaction solution was composed of 10 μM of an IsdG–heme sample in 20 mM Tris pH 7.4, 50 mM NaCl, 0.5 μL catalase, 1 mM EDTA and 1 mM sodium ascorbate. Due to ascorbate's high reactivity, ascorbate was added to the reaction last. The rate of heme degradation by each variant was monitored by Abs spectroscopy starting immediately after adding the ascorbate for every 5 min for 170 min from 800 to 350 nm using a Cary 100 Bio spectrophotometer with a scan rate of 600 nm/min, bandwidth of 2 nm, averaging time of 0.1 s, and a data interval of 1 nm. The activity measured in the presence of SOD involved the same

reaction except that 90 units/mL of SOD were added to the solution before adding 1 mM ascorbate. All assays were run at room temperature. The pseudo-first-order rate constant of heme degradation by each species was determined by fitting the decrease in the Soret band absorbance at 412 nm to an exponential decay using GraphPad Prism.

Liquid chromatography-mass spectrometry (LC-MS) was used to determine the composition of the products formed by the heme degradation reaction catalyzed by W67F IsdG. The LC-MS analysis was performed on a Shimadzu Prominence HPLC instrument coupled to an ABI Sciex 4000 QTrap Pro mass spectrometer operated in positive ion mode. The samples were loaded on a Jupiter C-18 column (150 x 1 mm; 5 μm, Phenomenex) at a flow rate of 80 μL/min. The following conditions were used for the W67F IsdG–heme sample with SOD: 1 min, 2%B; 1-15 min, 98%B; 15-20 min, 98%B; 20-20.01 min, 2%B, 20.01-35 min, 2%B. Similar conditions were used for the W67F IsdG–heme sample without SOD: 2 min, 2%B; 2-33 min, 98%B; 33-35.99 min, 98%B; 35.99-36 min, 2%B, 36-50 min, 2%B. For each sample, solvent A was 0.1% formic acid in water and solvent B was 0.1% formic acid in acetonitrile. Electrospray conditions in a positive ion mode with a capillary voltage 5500V at 400 ºC. W67F IsdG–heme with SOD was analyzed in the Q1 scanning mode at a scan speed of 250 m/Z sec over a range of 250 to 1000 m/Z. W67F IsdG–heme without SOD was analyzed in the Q3, linear ion trap, scanning mode at a scan speed of 1000 m/Z sec over a range of 250 to 1000 m/Z with a collision energy fixed at 5 V. The Q3 scanning mode was used instead of the Q1 scanning mode to improve the resolution of the peaks in the chromatogram of the sample of W67F IsdG–heme without SOD. This was not necessary for the sample of W67F IsdG–heme with SOD.

RESULTS

Activity Assays

CD Assays. UV CD spectroscopy was used to gain insight into changes to the secondary structure of IsdG as a result of the W67A and W67F substitutions. These data provided an assessment of whether any enzyme activity changes could be attributed to protein secondary structure changes. UV CD data were collected and compared between WT and W67A IsdG (Figure 7) and between WT and W67F IsdG–heme (Figure 8). The spectra were analyzed using the CDSSTR program by Dicroweb. The algorithm used by this program quantified the proportions of α-helices and β-sheets in each variant of IsdG. The CDSSTR program fit the experimental and reconstructed data better than any other program by Dicroweb.

The W67A and WT IsdG spectra in Figure 7 were significantly different in shape, especially compared to that of W67F and WT IsdG–heme in Figure 8. This indicated that there were significant differences between the secondary structures of WT and W67A IsdG, so it would be impossible to distinguish whether any changes in activity of W67A IsdG are the result of the differences in the enzymes' secondary structure or of second-sphere interactions within the enzyme active site. Therefore, no further spectroscopic analysis was conducted on W67A IsdG.

On the other hand, the WT and W67F IsdG–heme spectra were very similar in shape, with slightly more intense peaks observed in the W67F IsdG–heme spectrum. The ratio of these secondary structural elements calculated by CDSSTR were compared to quantify the similarity of two proteins' secondary structures. W67F IsdG–heme contained 2% more α-helices and 1% less β-sheets than WT IsdG–heme. Apo W67F IsdG contained 2% less α-helices and 3% more β-sheets than apo WT IsdG. Each of these differences were below the range of RMSD values of 0.065 to 0.070, which were determined for this program in a previous study.[21] This indicated that there

were no significant differences between the secondary structures of WT and W67F IsdG–heme, so any changes to the activity observed by W67F IsdG were attributed to changes in second-sphere interactions within the enzyme active site.

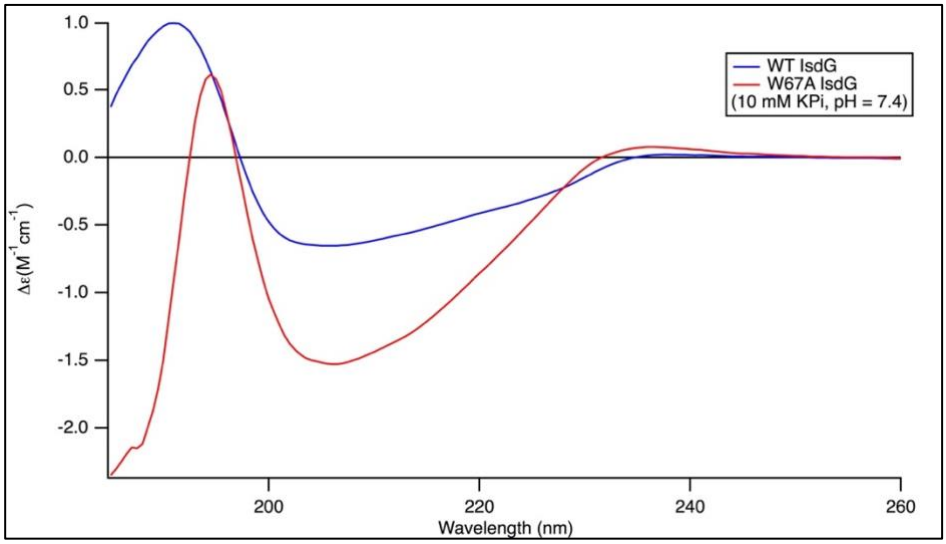

Figure 7. UV CD spectra of Apo W67A (red) and WT (blue) IsdG in 10 mM KPi pH 7.4. The significantly different spectra indicate that there were significant changes to the secondary structure of IsdG as a result of the amino acid substitution.

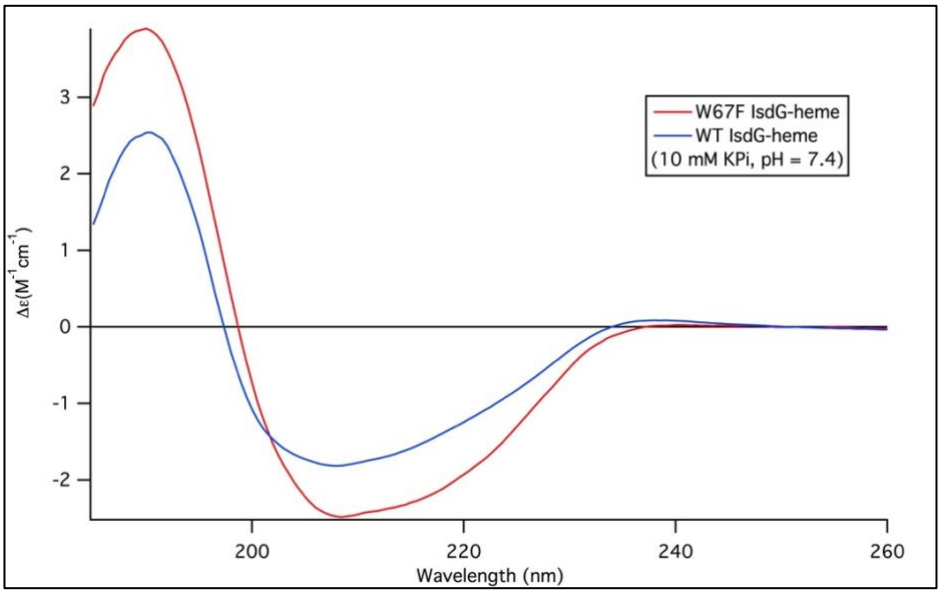

Figure 8. UV CD spectra of W67F (red) and WT (blue) IsdG–heme in 10 mM KPi pH 7.4. Through analysis of the spectra with CDSSTR, it was determined that there were no significant changes to the secondary structure of IsdG, despite the amino acid substitution.

Abs Assays. While the activity of W67F IsdG had not been previously studied, the W67A variant resulted in a loss of activity in a previous study.[14] Likewise, the W66F variant of IsdI, which involved the same substitution to IsdI's analogous Trp residue, resulted in reduced enzyme activity.[16] Thus, it was hypothesized that the substitution of the Trp residue in IsdG to a smaller residue, Phe, would result in reduced enzyme activity as well. To test this, ascorbate-catalyzed degradation of heme was monitored spectrophotometrically every 5 min for 170 min. Catalase was added to all solutions at the start of the reaction to eliminate the possibility for any free hydrogen peroxide in the solution to cause heme degradation.[23] The Soret band at 412 nm, representing the IsdG protein bound to heme in a 1:1 heme to protein ratio, shows a clear decrease over the entire period in both the WT (Figure 9) and W67F IsdG–heme (Figure 10) spectra. This indicates that the enzyme is still active, despite the substitution of the active site residue. There was also a small peak that increased overtime at approximately 680 nm in the W67F IsdG spectra in the absence of SOD, which has been cited to be consistent with biliverdin formation (Figure 10).[6]

Activity assays were done in both in the presence and absence of SOD, an enzyme that catalyzes the dismutation of any superoxide radicals into hydrogen peroxide and molecular oxygen. Any hydrogen peroxide produced in this process is decomposed by catalase into water and oxygen to prevent it from causing oxidative damage. The addition of SOD did not appear to alter the shape of the WT spectra (Figure 9), while it did alter the shape of the W67F IsdG–heme spectra (Figure 10). The W67F spectra in the presence of SOD, on the right of Figure 10, contained less intense peaks at longer wavelengths after the Soret peak at 412 nm through 500 nm, illustrating a clearer conversion of IsdG–heme into products.

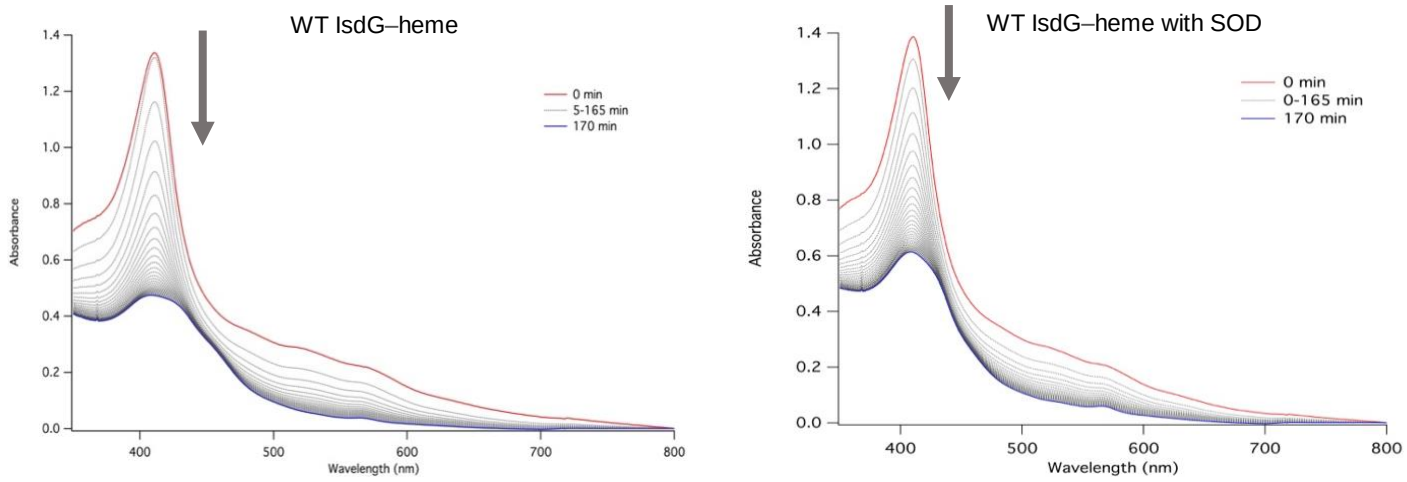

Figure 9. Abs activity data for the reaction of WT IsdG–heme with ascorbate. The assay consisted of 10 μM WT IsdG–heme in 20 mM Tris pH 7.4, 50 mM NaCl, 1 mM ascorbate, 1 mM EDTA and 0.5 μL catalase. For the reaction in the presence of SOD, 0.03 mg SOD was added to the solution. Spectra were taken every 5 min for 170 min. Both spectra also show a reduction of the IsdG–heme Soret band at ~412 nm over time, indicating that WT IsdG is active.

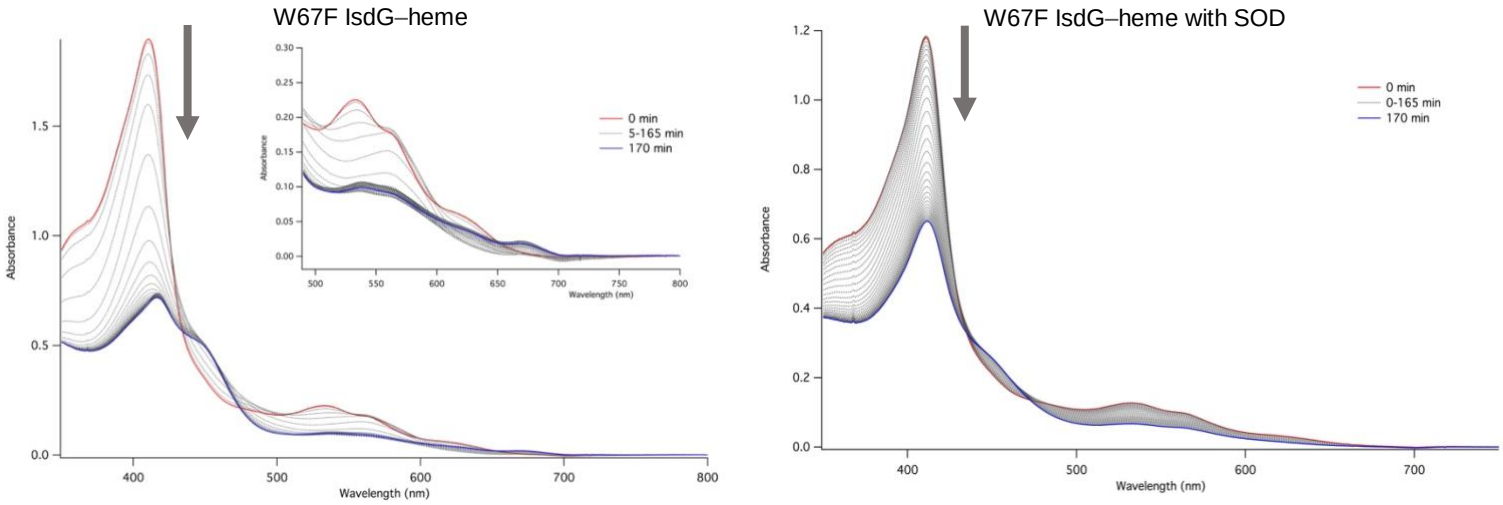

Figure 10. Abs activity data for the reaction of W67F IsdG–heme with ascorbate. The assay consisted of 10 μM W67F IsdG–heme in 20 mM Tris pH 7.4, 50 mM NaCl, 1 mM ascorbate, 1 mM EDTA and 0.5 μL catalase. For the reaction in the presence of SOD, 0.03 mg SOD was added to the solution. Spectra were taken every 5 min for 170 min. Both spectra show a reduction of the IsdG–heme Soret band at ~412 nm and a decreasing Q band at ~530 nm over time, suggesting that W67F IsdG–heme is active.

From the activity assay data, the rate constants of WT and W67F IsdG-catalyzed heme degradation in the presence and absence of SOD were calculated to better compare the relative activities of each enzyme. The pseudo-first-order rate constants for WT and W67F in the presence of SOD were 0.0369 ± 0.0019 and 0.0166 ± 0.0046 min^{-1}, respectively. The rate constants for WT and W67F in the absence of SOD were 0.0414 ± 0.0036 and 0.0399 ± 0.0088 min^{-1}, respectively. In both cases the rate constant of W67F IsdG was smaller than that of WT IsdG. Additionally, the rate constants of both WT and W67F IsdG decreased upon the addition of SOD. The rate constant of W67F IsdG in the absence of SOD was greater than double the rate constant of W67F IsdG in the presence of SOD. This suggested that a non-enzymatic reaction is predominant in the absence of SOD.

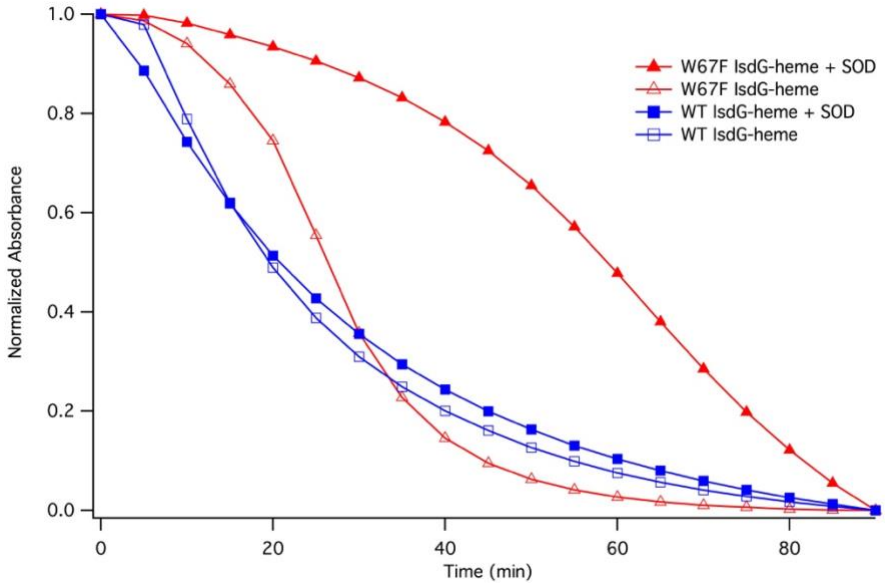

Figure 11. IsdG-catalyzed heme degradation assays fit to first order rate laws. The pseudo-first-order rate constants for WT and W67F IsdG in the presence of SOD were determined to be 0.0369 ± 0.0019 and 0.0166 ± 0.0046 min^{-1}, respectively. The rate constants for WT and W67F in the absence of SOD were 0.0414 ± 0.0036 and 0.0399 ± 0.0088 min^{-1}, respectively.

The W67F samples containing catalase in the absence and presence of SOD were analyzed using LC-MS in positive ESI (Figure 12). Each chromatogram contained a peak at m/Z of about

12,700 that represented the protein (MW 12,700 Da), a peak at m/Z of about 616 that represented heme (MW 616 Da) (Figure 12B,D) and at m/Z of about 583 that represented biliverdin (MW 582 Da) (Figure 12A,C). The intensity of the peak representing biliverdin in the chromatogram of the W67F IsdG–heme in the presence of SOD (Figure 12C) was much smaller than that in the absence of SOD (Figure 12A), suggesting that much less biliverdin was produced by W67F IsdG in the presence of SOD. The heme degradation reaction by W67F IsdG did not appear to produce any bilirubin (MW 584 Da) or staphylobilin (MW 598 Da), evident by the lack of peaks corresponding to these compounds in the chromatograms.

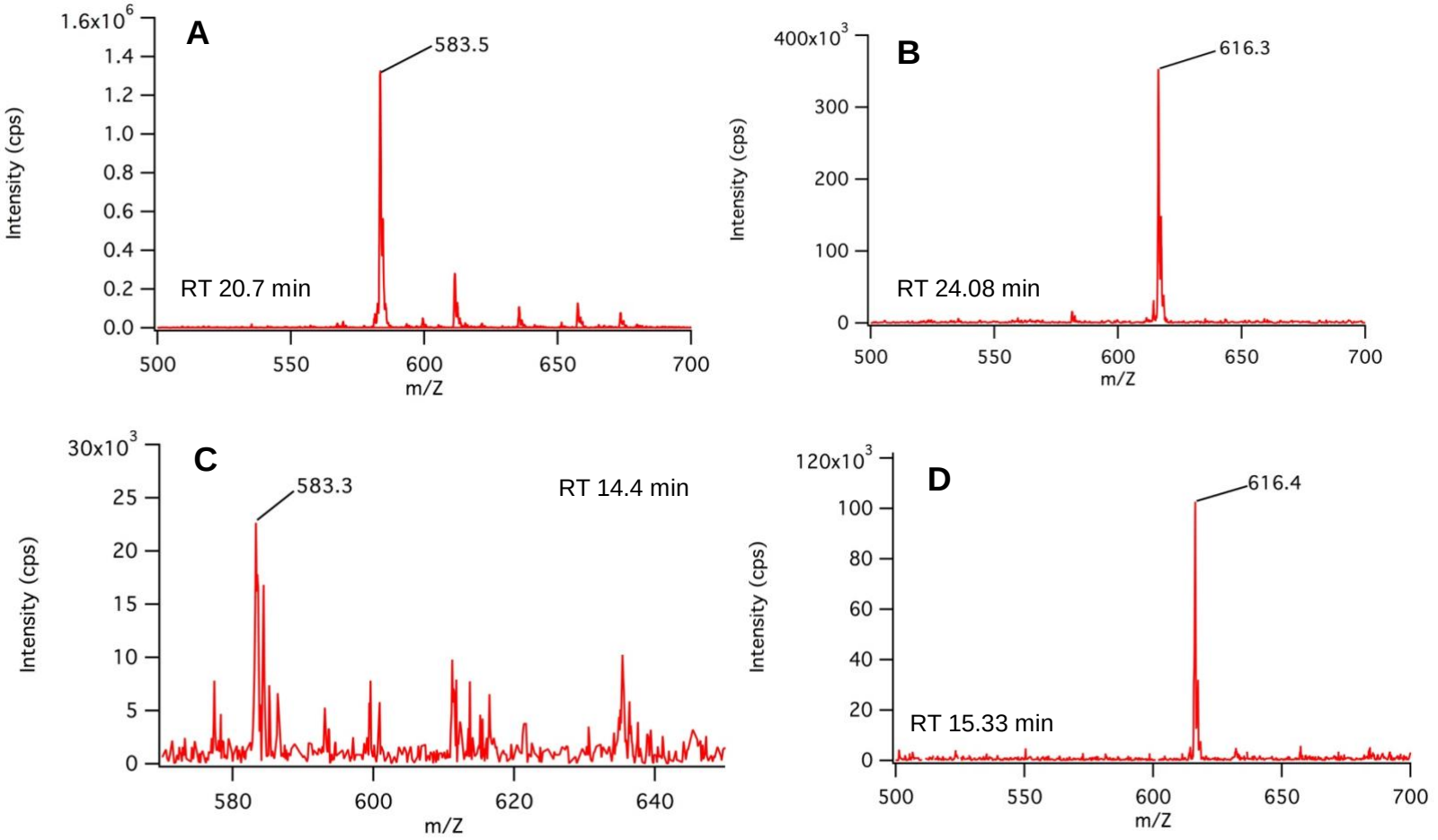

Figure 12. ESI LC-MS of W67F IsdG–heme degradation assay products in the absence (A, B) and presence of SOD (C, D). A) Protonated molecular ion of biliverdin with MW 582 Da, B) Charged molecular ion of heme with MW 616 Da, C) Protonated molecular ion of biliverdin in presence of SOD, D) Charged molecular ion of heme in presence of SOD. No bilirubin, MW 584 Da, or staphylobilin, MW 598, was detected.

Abs Spectroscopy

Abs Data. Abs data were collected and compared between WT and W67F IsdG–heme–CN to understand how the W67F substitution affected the extent of porphyrin ruffling by IsdG. The effect was determined by comparing the energies of the Q and Soret bands in the two spectra produced by UV-Vis analysis. The W67F IsdG–heme–CN Q and Soret bands each blue-shifted to higher energy by about 100 cm^{-1}. The Q band shifted to 18,100 cm^{-1} from 18,000 cm^{-1} in WT IsdG and the Soret band shifted to 23,900 cm^{-1} from 23,800 cm^{-1} in WT IsdG (Figure 13).

The energy values of the Q and Soret bands were analyzed using the PBE/TZVP TDDFT-predicted Abs spectra from a previous study of cyanide- and imidazole-ligated low-spin ferric heme.[18] Figure 5 illustrates the dependence of the Q and Soret band energies on heme ruffling. The general trend predicted by this model is that at small distortions, increased ruffling triggers no change to the Q band and a blue-shift of the Soret. At larger distortions, increased ruffling triggers red-shifts of both the Q and Soret bands. A previous study determined that WT IsdG–heme–CN results in 2.04 Å of ruffling based on QM/MM calculations.[24] This model indicates that because the Q and Soret band both blue-shift with the same magnitude, the W67F IsdG–heme–CN results in greater than 1.0 Å of ruffling. The fact that both the Q and Soret band of W67F IsdG–heme–CN blue-shift from that of the WT IsdG–heme–CN indicates reduced heme ruffling in this variant. Based on the analysis within the study that proposed this model, it is estimated that W67F IsdG–heme–CN results in 1.7 Å of ruffling.[18] This data supported the original hypothesis that the substitution of Trp67 by a smaller residue would result in reduced porphyrin ruffling.

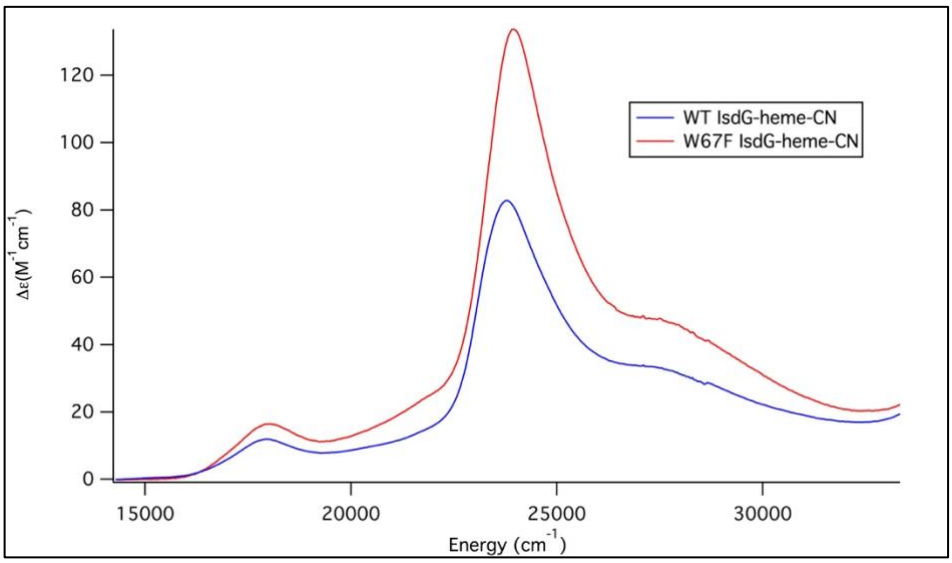

Figure 13. Abs spectra of WT (blue) and W67F (red) IsdG–heme–CN in 150 mM NaCl, 50 mM Tris pH 7.4. The W67F Q and Soret bands each blue-shift 100 cm^{-1}, to higher energy with decreased steric bulk at residue 67, indicating reduced porphyrin ruffling.

MCD Spectroscopy

MCD Data. MCD spectroscopy was used to investigate differences between the electronic structures of W67F and WT IsdG–heme–CN. MCD data was collected on W67F and WT IsdG–heme–CN at higher (Figure 14) and lower energies (Figure 15), both of which provided insight into heme electronic structure. The data collected at lower energies were acquired using samples of higher concentrations of W67F and WT IsdG–heme–CN for better visualization of the weaker Q bands. The shapes and locations of the Soret (Figure 14) and Q bands (Figure 15) were compared between each spectrum. Overall, the two spectra were very different and the W67F IsdG–heme–CN spectrum contained more intense peaks than the WT IsdG–heme–CN spectrum. The most intense spectral feature is the negative component of the Soret band in the W67F IsdG–heme–CN spectrum (Figure 13). The negative Soret peak blue-shifted by about 100 cm^{-1} in the W67F IsdG–heme–CN spectrum from 23,500 cm^{-1} in the WT IsdG–heme–CN spectrum to 23,600 cm^{-1}, which is consistent with the shift seen in the Abs spectra for WT and W67F IsdG–heme–CN (Figure 13). The two spectra have the same zero-crossing point for the Soret band of about 24,200 cm^{-1}. The low energy region in the W67F IsdG–heme–CN spectra has similar peaks to the WT spectra. WT IsdG–heme–CN had four positively signed bands at 16,800, 18,200, 19,700, and 21,700 cm^{-1} and a negatively signed band at 17,600 cm^{-1}. W67F IsdG–heme–CN had three positively signed bands at 16,700, 19,700 and 21,800 cm^{-1} and two negatively signed bands at 17,600 and 18,400 cm^{-1} (Figure 15). While most of these peaks were more intense in the W67F IsdG–heme–CN spectrum, the peak on the W67F spectrum at around 18,000 cm^{-1} was much less intense than the peak in that location on the WT spectrum. Overall, the introduction of the W67F substitution did not cause any bands to shift by more than 100 cm^{-1} for IsdG–heme–CN (Figures 14-15). However, the

differences in intensities suggest that the electronic structures of W67F and WT IsdG–heme–CN are different.

The significant increase in the intensity of the negatively-signed Soret band in the W67F IsdG–heme–CN spectrum observed in Figure 14 is the most apparent change in the spectra. This observation is consistent with an increased population of the ^2E_g electronic state in W67F IsdG seen in MCD data from other heme-binding enzymes.[17-18] The intensity of the *C*-term of the ^2E_g electronic state can increase as a result of spin-orbit coupling (SOC) between the two components of the ^2E_g electronic state.[18]

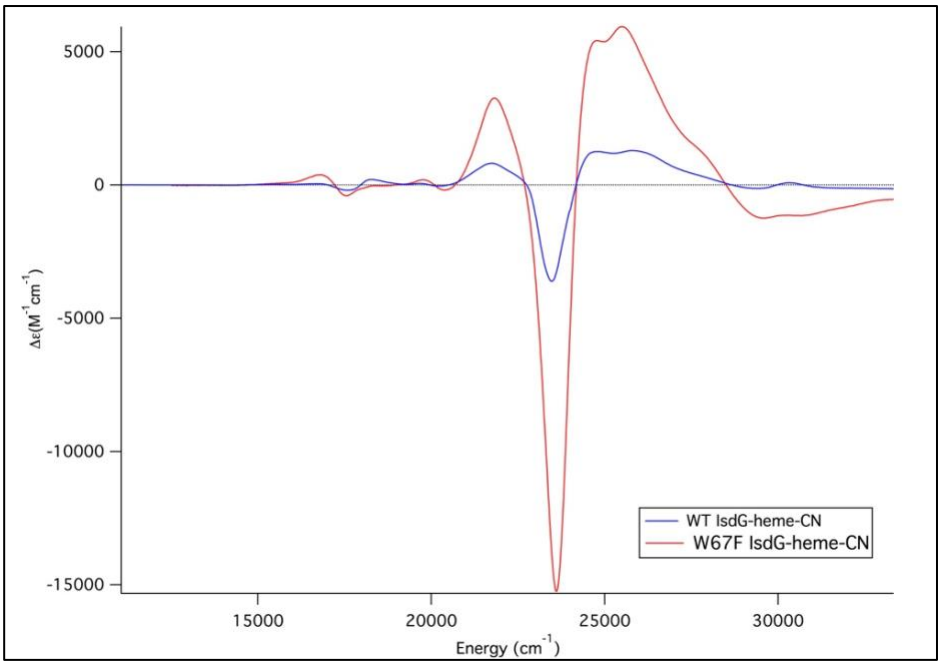

Figure 14. MCD spectra of 10 μM WT and W67F IsdG–heme-CN in 50 μM KPi pH 7.4, 60% (*v/v*) glycerol at 7 T, 5 K. The MCD spectrum of W67F IsdG–heme–CN is significantly different from that of WT IsdG–heme–CN, confirming that the electronic structure has been altered by the substitution. The W67F spectra contains more intense peaks than the WT spectra and the negative component of the Soret in the W67F spectra is significantly increased consistent with a transition from $^2B_{2g}$ to ^2E_g ground state.

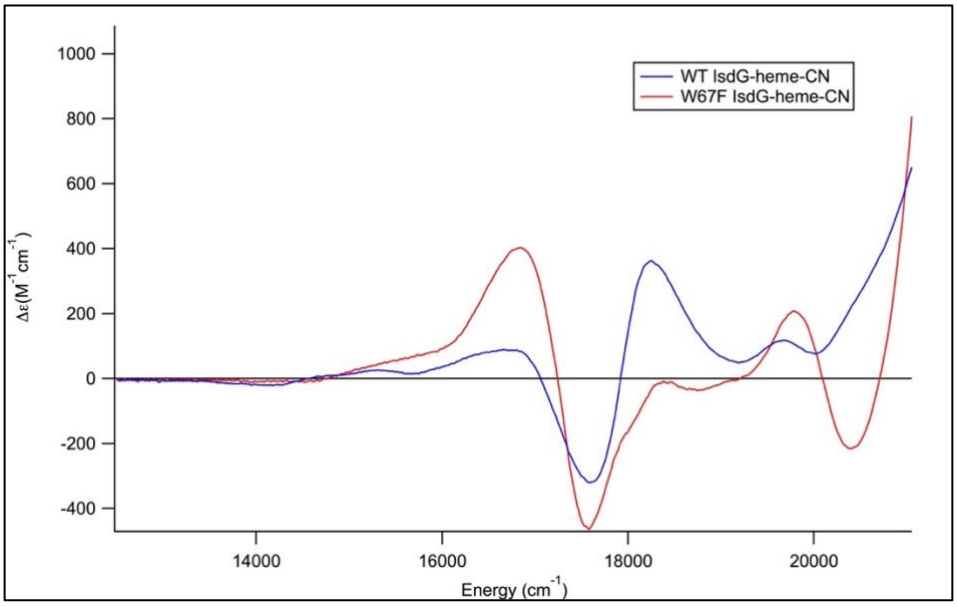

Figure 15. Low energy MCD spectra of 100 μM WT and W67F IsdG–heme-CN in 50 μM KPi pH 7.4, 60% (*v/v*) glycerol at 7 T, 5 K. The intensities of the peaks are different between the two spectra, but the peaks do appear at similar energies.

DISCUSSION

Abs, UV CD and MCD spectroscopy together provided insight into the influence of Trp67 on the geometric and electronic structure of the IsdG protein. Previous studies have shown that active site residues of nCHOs, such as IsdG, are involved in heme ruffling and affect the electronic structure and reactivity of the heme complex.[15-18] This investigation gained insight into the contribution of Trp67 on heme ruffling, which has been seen to directly contribute to heme ruffling as a result of the steric contact it forms with the β-*meso* carbon in heme (Figure 4C).[14] As previously mentioned, heme ruffling is one of the most striking differences between the heme degradation reactions by IsdG and canonical HOs. Therefore, it was expected that the substitution of Trp67 with smaller residues, Ala and Phe, would result in reduced heme ruffling and IsdG activity.

Geometric Structure Changes to W67F IsdG

The CD spectra of WT and W67A IsdG were significantly different, indicating that the two enzymes had significantly different geometric structures (Figure 7). These differences make it impossible to conclude whether changes in enzyme activity were the result of the change to second-sphere interactions. This was because such changes could also be the result of the different protein secondary structures. Therefore, further analysis was not conducted on W67A IsdG, and instead the investigation focused on W67F IsdG.

The similarities between the WT and W67F IsdG–heme CD spectra indicated that the two enzymes had significantly similar geometric structures. Therefore, any changes in enzyme activity were concluded to be the result of second-sphere interactions (Figure 8). More specifically, any changes in enzyme activity were attributed to the substitution of Trp67 with Phe. The rate constants calculated from the activity assays of W67F IsdG were found to be smaller than those of WT IsdG, indicating that W67F IsdG had reduced activity compared to WT IsdG, as was hypothesized.

Each assay of WT and W67F IsdG included a decreasing Soret band at 412 nm, which was indicative of a decreasing concentration of the IsdG–heme complex. In previous studies, activity assays of WT IsdG under similar conditions showed the peak at 412 nm disappearing into a flat line at the final time point, indicating that all IsdG–heme had reacted.[6] However, this experiment did not show the same result over the course of 170 min. Instead, there appeared to be IsdG–heme remaining in solution, evident by the remaining peak at 412 nm (Figure 9). This could have been the result of the reaction using up all of the dissolved O_2, one of the main reactants required for the heme degradation reaction. Another explanation for this difference could have been due to the fact that the assays were carried out at room temperature, rather than at a higher temperature as was done by other studies.[6, 18] A higher temperature would have been expected to accelerate the

reaction in which WT IsdG–heme assays would go to completion at a faster rate than the W67F IsdG–heme reaction would. This finding would have confirmed that the W67F IsdG enzyme had reduced activity compared to that of WT IsdG, as the results from this investigation suggest.

Moreover, the presence of SOD in the WT IsdG–heme assay (Figure 9) did not significantly change the shape of spectra as it had in the W67F IsdG–heme assay (Figure 10). In the absence of SOD, peaks at about 450 and 680 nm increased in intensity over time in the W67F IsdG–heme assay. However, in the presence of SOD these peaks were hardly present (Figure 10). The rate constant calculated for the reaction of W67F IsdG was significantly smaller when in the presence of SOD (Figure 11). SOD is known to react with superoxide to prevent oxidative damage to the cell. Therefore, this finding suggested that there was a non-enzymatic reaction involving superoxide taking place in the absence of SOD. Thus, disrupting heme ruffling through the substitution of Trp67 had resulted in the production of a toxic reactive oxygen species, superoxide, which would have a toxic effect on the cells of *S. aureus*.

Another significant finding from the activity assays was the presence of a peak on the W67F IsdG spectra at 680 nm. A peak at 680 nm has been noted in previous studies to be indicative of the presence biliverdin, the product of heme degradation by canonical HOs.[6] The presence of biliverdin was confirmed with LCMS, which was used to compare the identity and amounts of products resulting from the degradation assays of W67F IsdG–heme in the presence and absence of SOD. Peaks representing heme (Figure 12B,D) and biliverdin (Figure 12A,C) were identified products of the W67F IsdG–heme assay both with and without SOD. However, the peak representing biliverdin was much less intense in the chromatogram of the assay in the presence of SOD (Figure 12C). This indicated that less biliverdin was formed by the reaction and less heme was degraded by W67F IsdG in the presence of SOD. This finding was consistent with the results

of the activity assay, in which the rate constant of W67F IsdG decreased as a result of the addition of SOD.

Moreover, biliverdin was an unusual product of this reaction and has not been noted to be produced by other variants of IsdG. Biliverdin is the known primary product produced through heme degradation by canonical HOs. Staphylobilin is the known primary product of heme degradation by IsdG, however, this product was not detected in the assay solution.[11] This suggested that the reaction catalyzed by W67F IsdG–heme proceeded through a unique reaction mechanism that differed from that of WT IsdG–heme, resulting in the production of biliverdin rather than staphylobilin. A similar result was found in a study involving the R26S variant of MhuD. MhuD, the heme degrading enzyme used by *Mycobacterium tuberculosis*, degrades heme into mycobilin and iron. However, the R26S variant of MhuD degraded heme into biliverdin instead.[25] For future studies, it would be worthwhile to determine if the substitution of the analogous Trp residues to Phe in MhuD and IsdI, other nCHOs, also yields biliverdin. Overall, this finding provided further insight into the role of Trp67 in the heme degradation mechanism of IsdG.

Further, Abs data collected on WT and W67F IsdG–heme–CN indicated reduced heme ruffling by W67F IsdG. Being that heme ruffling is important for IsdG activity, the results from the Abs data are consistent with the reduced activity of W67F IsdG from the W67F IsdG–heme observed from the activity assays. This finding also confirms that Trp67 is directly involved in heme ruffling as a result of the steric interaction it forms with the β- or δ-*meso* carbon within heme to push them out of the heme plane and toward the oxygen binding site.[14]

Electronic Structure Changes to W67F IsdG

The MCD data collected provided additional information to that collected by Abs spectroscopy regarding the electronic structure differences between WT and W67F IsdG–heme–CN. The blue-shift observed for the Soret band in the Abs spectrum of W67F IsdG–heme–CN (Figure 13) was consistent with the shift observed in MCD spectrum for this species compared to that of WT IsdG–heme–CN (Figure 14). The most striking difference between the two MCD spectra was the increased intensity of the negatively-signed Soret band of the W67F IsdG–heme–CN spectrum (Figure 14). This suggested that W67F IsdG–heme–CN that has a ^2E_g electronic ground state that has a $(d_{xy})^2 (d_{xz}, d_{yz})^3$ electron configuration (Figure 16). This differs from the $^2B_{2g}$ electronic ground state reported for WT IsdG–heme–CN that has a $(d_{xz}, d_{yz})^4 (d_{xy})^1$ electron configuration (Figure 17).[17-18] The symmetry between the d_{xz} and d_{yz} orbitals in the ^2E_g state allows the orbitals to rotate into each other resulting in increased spin orbit coupling (SOC), enabling degenerate states to have different energies in the presence of a magnetic field. The SOC observed between the two components of the ^2E_g state increased the intensity of the *C*-term in the MCD spectrum, resulting in the increased intensity observed for the negative Soret band of the W67F IsdG–heme–CN (Figure 14). On the other hand, the $^2B_{2g}$ state of WT IsdG–heme–CN lacked the unpaired electron in the d_{xz} and d_{yz} orbitals (Figure 17) that contributes to the *C*-term intensity, and therefore, the Soret peak is significantly less intense in the WT IsdG–heme–CN spectrum (Figure 14).

In the ^2E_g ground state an unpaired electron is located in the d_{xz} and d_{yz} orbitals (Figure 16), whereas in the B_{2g} ground state the unpaired electron is located in the d_{xy} orbital (Figure 17). The reduced heme ruffling observed by W67F IsdG–heme–CN has been seen to trigger the electronic change from the $^2B_{2g}$ state to the ^2E_g state. The reduced amount of heme ruffling reduces the

amount of unpaired electron density on the *meso* carbons of heme. This was consistent with the electron configuration in the ^2E_g state in which the unpaired electron is located in the degenerate d_{xz} and d_{yz} orbitals. On the other hand, the increased amount of heme ruffling by WT IsdG–heme–CN results in greater unpaired electron density placed on the *meso* carbons of heme. This was consistent with the electron configuration in the $^2B_{2g}$ state in which the unpaired electron is in the d_{xy} orbital. Greater ruffling facilitates the self-hydroxylation of heme that is involved in the mechanism of heme degradation by WT IsdG.[26] However, as previously stated, in the ^2E_g ground state the unpaired electron is located in the degenerate d_{xz} and d_{yz} orbitals rather than in the d_{xy} orbital. As a result, less of the unpaired electron density is placed on the *meso* carbons of heme and less heme ruffling is observed in the W67F IsdG–heme–CN complex. The ^2E_g ground state has been observed for canonical HOs, which also exert less heme ruffling compared to WT IsdG.[18]

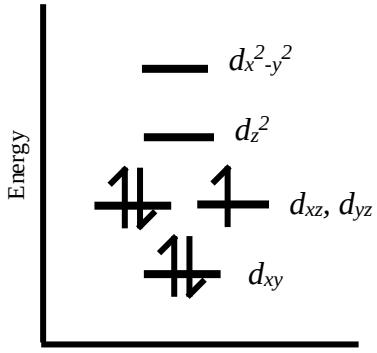

Figure 16. MO Diagram of the ^2E_g electron configuration of W67F IsdG–heme based on the MCD data. The intense negative Soret band in the MCD spectra results from significant SOC between the d_{xz} and d_{yz} orbitals that does not occur in the $^2B_{2g}$ state.

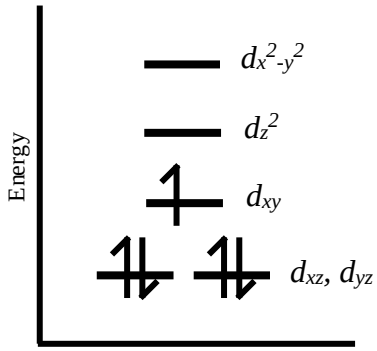

Figure 17. MO Diagram of the $^2B_{2g}$ electron configuration of WT IsdG–heme as reported by previous studies.[14-15] There is less SOC between d_{xy} and the other orbitals resulting in the reduced MCD intensity compared to that of the ^2E_g state.

A previous study used MCD spectroscopy to analyze the electronic structure of WT and W66F MhuD, which involved the same substitution to the analogous Trp residue in MhuD. The MCD spectra of W67F IsdG–heme–CN (Figures 14-15), WT MhuD–heme–CN and W66F MhuD–heme–CN at 5 K, 7 T (Figure 18) had similar shapes. The shapes and intensities of the peaks within the W67F IsdG–heme–CN and WT MhuD–heme–CN spectra were most similar.[18] At lower energy, both the WT and W66F MhuD–heme–CN spectra contained a negatively signed band followed by three positively signed bands. The energies of the bands differed slightly between the two proteins. The positive bands in the WT MhuD–heme–CN spectrum were at about 18,600, 19,500 and 22,000 cm^{-1} and those in the W66F MhuD–heme–CN spectrum were at 18,300, 19,500 and 21,599 cm^{-1} (Figure 18). The W67F IsdG–heme–CN spectrum was slightly different in that there was a negatively signed band followed by only two positively signed bands at 19,700 and 21,800 cm^{-1} (Figure 15). These positively signed bands appeared at slightly higher energies with a blue-shift of about 200 cm^{-1}, compared to those in the W66F MhuD–heme–CN spectrum. Moreover, the negative component of the Soret band was also the most intense spectral feature of the WT and W66F MhuD–heme–CN spectra as it was in the W67F IsdG–heme–CN spectrum. However, the energy of the negative Soret band in the WT MhuD–heme–CN spectrum at about

23,500 cm^{-1} was more similar to that of the negative Soret band in the W67F IsdG–heme–CN spectrum at about 23,600 cm^{-1}. The differences observed between the Q and Soret bands in the WT and W66F MhuD–heme–CN spectra by this previous study were attributed to a transition from the $^2B_{2g}$ state to a ^2E_g state, which was consistent with the findings regarding WT and W67F IsdG–heme–CN.[18]

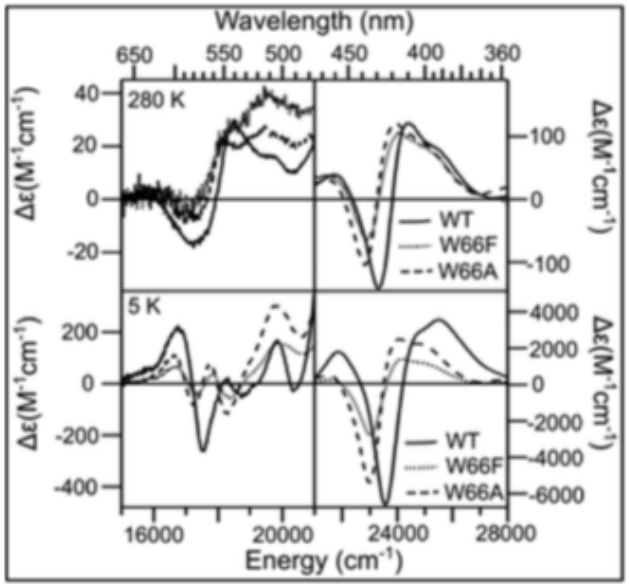

Figure 18. MCD spectra of WT (solid line), W66F (dotted line), and W66A (dashed line) MhuD–heme–CN at 280 (top) and 5 K (bottom), 7 T in 50 mM KPi pH 7.4, 50 mM NaCl, 60% (*v/v*) glycerol. The features of the WT MhuD spectrum are similar to those of the W67F IsdG–heme–CN spectrum observed in Figures 14-15. Adapted from Ref #18.

Similarly, MCD spectroscopy was used to analyze the electronic structure of WT IsdI–heme–CN at 5 K, 7 T (Figure 19B).[27] This spectrum was similar to that of WT IsdG–heme–CN, which has a very similar active site structure (Figures 14-15). The study on WT IsdI–heme–CN concluded that the MCD data strongly suggested a $^2B_{2g}$ state, as was the case for the data collected on WT IsdG–heme–CN and WT MhuD–heme–CN.[18]

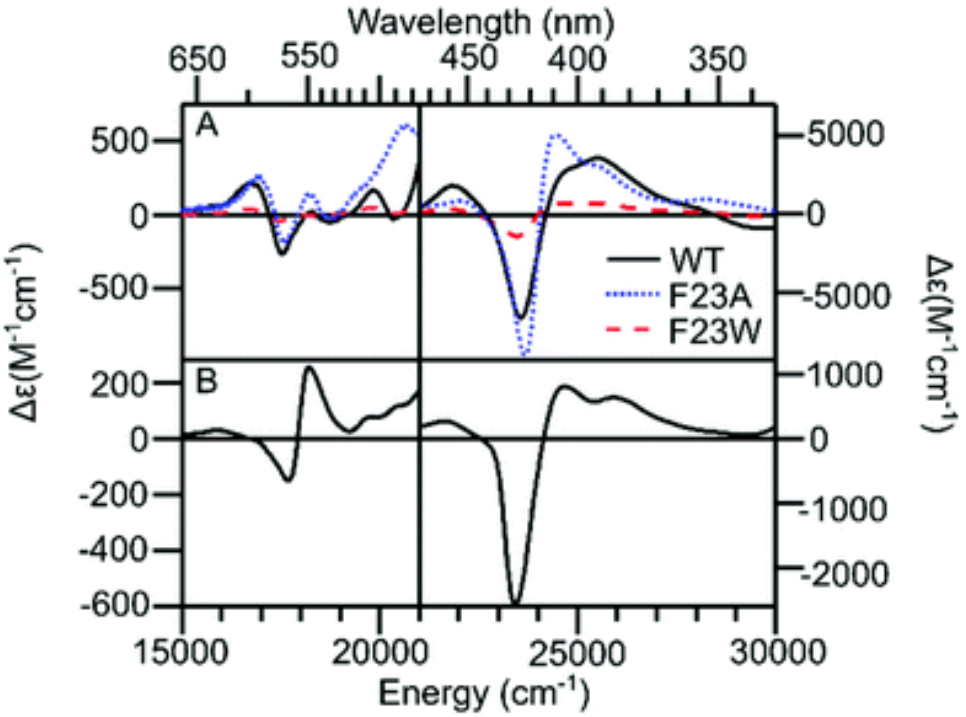

Figure 19. MCD spectra of WT MhuD–heme–CN (A, solid black), F23A MhuD–heme–CN (A, dotted blue), F23W MhuD–heme–CN (A, dashed red), and WT IsdI–heme–CN (B, solid black) at 5 K , 7 T in 50 mM KPi pH 7.4, 50 mM NaCl, 60% (*v/v*) glycerol. The features of the WT IsdI spectrum are similar to those of the WT IsdG–heme–CN spectrum observed in Figures 14-15. Adapted from Ref #27.

Implications for the Design of a Small Molecule Inhibitor

This study provides further insight into the interaction between Trp67 and the heme porphyrin complex, information that is useful for the development of a new drug target to prevent the degradation of heme by IsdG. As previously mentioned, IsdG degrades heme to acquire iron which serves as an essential nutrient used to power the pathogenesis of *S. aureus*. Therefore, preventing the acquisition of iron from heme by IsdG would inhibit the bacterium's pathogenesis throughout the human host as a whole. A previous study found that IsdG binds heme with a very small dissociation constant, suggesting that the development of a competitive inhibitor to prevent their interaction would be less effective than the development of an uncompetitive inhibitor that binds to the enzyme-substrate complex to inhibit the interaction between Trp67 and heme.[4] The

nitrogen within the indole ring of Trp67 faces away from heme and toward a nitrogen within the backbone amide bond of Phe73 (Figure 20). Phe73 is further away from heme and does not form contacts to the substrate as Trp67 does. A small molecule containing hydrogen acceptor atoms, such as a carboxylic acid group, could form hydrogen bonds to the hydrogen bonded to the nitrogen atoms of both Trp67 and Phe73, due to their proximity to one another. Such an interaction would pull the indole ring of Trp67 away from heme up toward Phe73, disrupting the steric interactions that Trp67 forms with the substrate. Being that Trp67 has been shown to influence heme ruffling and the IsdG activity, disrupting its interaction with heme would thus inhibit the extent of heme ruffling and IsdG activity. Additionally, the disruption of the interaction was also seen to result in the production of a toxic reactive oxygen species, superoxide. Such findings indicate that Trp67 would serve as a useful drug target for inhibiting heme degradation by IsdG, required for the survival of *S. aureus* in a human host.

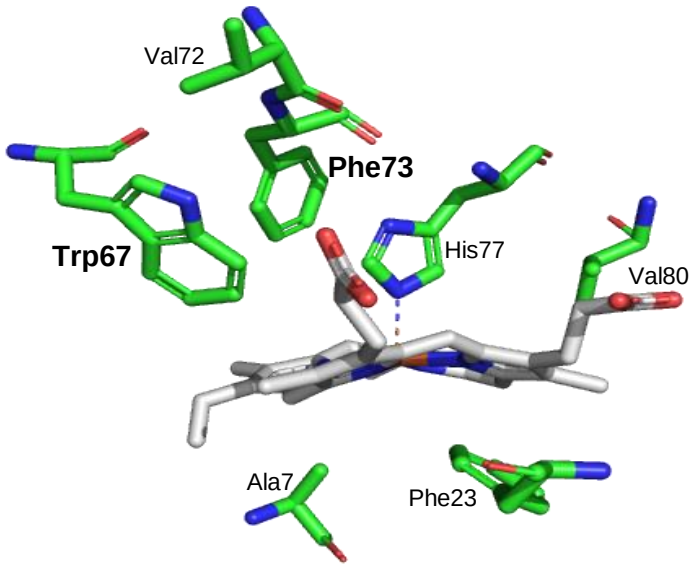

Figure 20. Location of Trp67 and Phe73 in the X-ray crystal structure of N7A IsdG–heme (PDB ID 2ZDO).[14] Trp67 forms a steric contact with heme contributing to heme ruffling. A potential uncompetitive inhibitor to this interaction could be a small molecule that forms hydrogen bonds to the Phe73 nitrogen in the amide bond and the Trp67 nitrogen within the indole ring, pulling the Trp67 indole ring away from heme (gray) and toward Phe73.

Conclusion

Overall, the findings from this investigation support the original hypothesis that the W67F substitution resulted in reduced enzymatic turnover and heme ruffling compared to WT IsdG. Thus, Trp67 has been confirmed to be involved in heme ruffling and enzymatic turnover by IsdG. Spectroscopic characterizations of WT and W67F IsdG–heme–CN have indicated that the second-sphere Phe residue does not introduce a geometric change to the IsdG enzyme, but does alter the electronic structure of the IsdG–heme complex. A significant finding of this study was that heme degradation assays of W67F IsdG–heme in the presence of ascorbate and catalase resulted in the formation of biliverdin, the product of the heme degradation reaction by canonical HOs, rather than staphylobilins, the product of the reaction by WT IsdG–heme. This suggested that the reaction catalyzed by W67F IsdG proceeded through a different reaction mechanism than that of WT IsdG, indicating that Trp67 plays a significant role in the heme degradation mechanism of IsdG. Together, the results of this spectroscopic investigation of IsdG provide further insight into the unique mechanism of heme degradation by IsdG and its differences from that of canonical HOs. Such information is highly useful for the development of a new therapeutic drug target specific to IsdG and its interaction with heme. A disruption to this interaction would inhibit the ability of IsdG to acquire iron from heme that is necessary for the pathogenesis of *S. aureus*, thus preventing further infection of the eukaryotic host by the bacterium.

Acknowledgements

I would like to thank my advisor, Professor Matt Liptak, who provided me with the incredible opportunity to gain experience working on in a research laboratory over the past three years. The success of this project was largely the result of the continuous support and insight that he had provided me throughout it. I am also very appreciative of the guidance given to me by graduate students Matt Conger and Ariel Shuelke, who collected a lot of the data used in this investigation. Their knowledge and patience throughout this project also largely contributed to my success with this project. I am thankful for the collaboration and feedback from other group members in the laboratory including Biswash Thakuri, Kayla Johnson, Jacob Morris, Aarzoo Grover, Adam Petrucci and Tanner James. I am also very grateful for the other two members of my Defense Committee for their contributions to my academic success beyond this project. I would like to thank Professor Silveira for teaching biochemistry with an unparalleled amount of enthusiasm, and for providing me the opportunity to utilize the knowledge that I acquired from his class in a meaningful way as a teaching assistant in his classroom. I would like to thank Professor Brewer for the extensive guidance that he provided me both as a professor and advisor over the past four years (and for always having an endless list of jokes on hand at the start of each class). Lastly, I would like to thank my family and friends, including Jon Haas, Nick Minadeo and Jenna Alessandro, for the motivation and support that they provided me over the past four years, especially toward the completion of this project. Each of the individuals listed above have largely contributed to my success throughout my time at the University of Vermont, and for that I am incredibly thankful. This thesis was further supported by a Summer Research Award from the Office of Undergraduate Research and Fellowships.

References

1. Klein, E. Y.; Mojica, N.; Jiang, W.; Cosgrove, S. E.; Septimus, E.; Morgan, D. J.; Laxminarayan, R., Trends in Methicillin-Resistant Staphylococcus aureus Hospitalizations in the United States, 2010-2014. *Clin. Infect. Dis.* **2017,** *65* (11), 1921-1923.
2. Prevention, C. f. D. C. a. Antibiotic Resistance Threats in the United States, 2013. https://www.cdc.gov/drugresistance/threat-report-2013/pdf/ar-threats-2013-508.pdf (accessed March 2019).
3. Levi, S.; Rovida, E., The role of iron in mitochondrial function. *Biochim. Biophys. Acta, General Subjects* **2009,** *17907* (629-636).
4. Conger, M. A.; Pokhrel, D.; Liptak, M. D., Tight binding of heme to Staphylococcus aureus IsdG and IsdI precludes design of a competitive inhibitor. *Metallomics* **2017,** *9*, 556-563.
5. Mazmanian, S. K.; Skaar, E. P.; Gaspar, A. H.; Humayun, M.; Gornicki, P.; Jelenska, J.; Joachmiak, A.; Missiakas, D. M.; Schneewind, O., Passage of Heme-Iron Across the Envelope of Staphylococcus aureus. *Science* **2003,** *299* (5608), 906-909.
6. Skaar, E. P.; Gaspar, A. H.; Schneewind, O., IsdG and IsdI, heme-degrading enzymes in the cytoplasm of Staphylococcus aureus. *J. Biol. Chem.* **2004,** *279*, 436-443.
7. Tiedemann, M. T.; Muryoi, N.; Heinrichs, D. E.; Stillman, M. J., Iron acquisition by the haem-binding Isd proteins in Staphylococcus aureus: studies of the mechanism using magnetic circular dichroism. *Biochem Soc T* **2008,** *36* (6), 1138-1143.
8. Yoshida, T.; Migita, C. T., Mechanism of heme degradation by heme oxygenase. *J. Inorg. Biochem.* **2000,** *82* (1-4), 33-41.

9. Wilks, A.; Schmitt, M. P., Expression and Characterization of a Heme Oxygenase (Hmu O) from Corynebacterium diphtheriae. *J. Biol. Chem.* **1998,** *273*, 837-841.

10. Loutet, S. L.; Kobylarz, M. J.; Chau, C. H. T.; Murphy, M. E. P., IruO Is a Reductase for Heme Degradation by IsdI and IsdG Proteins in *Staphylococcus aureus*. *J. Biol. Chem.* **2013,** *288* (36), 25749-25759.

11. Streit, B. R.; Kant, R.; Tokmina-Lukaszewska, M.; Celis, A. I.; Machovina, M. M.; Skaar, E. P.; Bothner, B.; DuBois, J. L., Time-resolved Studies of IsdG Protein Identify Molecular Signposts along the Non-canonical Heme Oxygenase Pathway. *J. Biol. Chem.* **2016,** *291*, 862-871.

12. Matsui, T., Nambu, S., Ono, Y., Goulding, C.W., Tsumoto, K., Ikeda-Saito, M., Heme degradation by Staphylococcus aureus lsdG and IsdI liberates formaldehyde rather than carbon monoxide. *Biochemistry* **2013,** *52*, 3025-3027.

13. Wu, R.; Skaar, E. P.; Zhang, R.; Joachimiak, G.; Gornicki, P.; Schneewind, O.; Joachimiak, A., Staphylococcus aureus IsdG and IsdI, Heme-degrading Enzymes with Structural Similarity to Monooxygenases. *J. Biol. Chem.* **2005,** *280*, 2840-2846.

14. Lee, W. C.; Reniere, M. L.; Skaar, E. P.; Murphy, M. E. P., Ruffling of Metalloporphyrins Bound to IsdG and IsdI, Two Heme-degrading Enzymes in *Staphylococcus aureus*. *J. Biol. Chem.* **2008,** *283* (45), 30957-30963.

15. Takayama, S. J.; Ukpabi, G.; Murphy, M. E. P.; Mauk, A. G., Electronic properties of the highly ruffled heme bound to the heme degrading enzyme IsdI. *Proc. Natl. Acad. Sci. USA* **2011,** *108* (32), 13071-13076.

16. Ukpabi, G.; Takayama, S. J.; Mauk, A. G.; Murphy, M. E. P., Inactivation of the Heme Degrading Enzyme IsdI by an Active Site Substitution That Diminishes Heme Ruffling. *J. Biol. Chem.* **2012,** *287* (41), 34179-24188.

17. Lockhart, C. L.; Conger, M. A.; Pittman, D. S.; Liptak, M. D., Hydrogen bond donation to the heme distal ligand of Staphylococcus aureus IsdG tunes the electronic structure. *J. Biol. Inorg. Chem.* **2015,** *20* (5), 757-70.

18. Graves, A. B.; Graves, M. T.; Liptak, M. D., Measurement of Heme Ruffling Changes in MhuD Using UV-vis Spectroscopy. *J. Phys. Chem.* **2016,** *120* (16), 3844-3853.

19. Lehnert, N., Elucidating second coordination sphere effects in heme proteins using low-temperature magnetic circular dichroism spectroscopy. *J. Inorg. Biochem.* **2012,** *110*, 83-93.

20. Kapust, R. B.; Tözsér, J.; Fox, J. D.; Anderson, D. E.; Cherry, S.; Copeland, T. D.; Waugh, D. S., Tobacco etch virus protease: mechanism of autolysis and rational design of stable mutants with wild-type catalytic proficiency. *Protein Eng.* **2001,** *14*, 993-1000.

21. Sreerama, N.; Woody, R. W., Estimation of Protein Secondary Structure from Circular Dichroism Spectra: Comparison of CONTIN, SELCON, and CDSSTR Methods with an Expanded Reference Set. *Anal. Biochem.* **2000,** *287*, 252-260.

22. Berry, E. A.; Trumpower, B. L., Simultaneous determination of hemes a, b, and c from pyridine hemochrome spectra. *Anal. Biochem.* **1987,** *161* (1).

23. Sigman, J. A.; Wang, X.; Lu, Y., Coupled Oxidation of Heme by Myoglobin is Mediated by Exogenous Peroxide. *J. Am. Chem. Soc.* **2001,** *123* (28), 6945-6946.

24. Conger, M. A.; Cornetta, A. R.; Liptak, M. D., Spectroscopic evidence for electronic control of heme hydroxylation by IsdG. *J. Am. Chem. Soc.* **2019,** *in preparation*.

25. Chao, A.; Goulding, C. W., A Single Mutation in the Mycobacterium tuberculosis Heme-Degrading Protein, MhuD, Results in Different Products. *Biochemistry* **2019,** *58* (6), 489-492.

26. Wilks, A.; Heinzl, G., Heme oxygenation and the widening paradigm of heme degradation. *Arch. Biochem. Biophys.* **2014,** *544*, 87-95.

27. Graves, A. B.; Horak, E. H.; Liptak, M. D., Dynamic ruffling distortion of the heme substrate in non-canonical heme oxygenase enzymes. *Dalton Transactions* **2016,** *45* (24), 10058-10067.

Supporting Information

Table S1. Long linker W67A primer

Primer	Sequence
Forward	5'-TGCTTTAAAGACATCAGATTTTAACGCATCCGTAAAAGCTTGCTTTGATTTC-3'
Backward	5'-GAAATCAAAGCAAGCTTTTACGGATGCGTTAAAATCTGATGTCTTTAAAGCA-3'

Table S2. Long linker W67F primer

Primer	Sequence
Forward	5'-GCTGCTTTAAAGACATCAGATTTTAAGAAATCCGTAAAAGCTTGCTTTG-3'
Backward	5'-CAAAGCAAGCTTTTACGGATTTCTTAAAATCTGATGTCTTTAAAGCAGC-3'

Table S3. W67A IsdG Gene Sequence including N-terminal His_6-tag, long-linker, and TEV cleavage site. The polypeptide begins at S-1, after the S219V TEV cleavage.

M-32	**G-31**	**H-30**	**H-29**	**H-28**	**H-27**	**H-26**	**H-25**	**D-24**	**Y-23**
ATG	GGT	CAT	CAT	CAT	CAT	CAT	CAC	GAT	TAC
D-22	**I-21**	**P-20**	**T-19**	**T-18**	**E-17**	**N-16**	**L-15**	**Y-14**	**F-13**
GAT	ATC	CCA	ACG	ACC	GAA	AAC	CTG	TAT	TTT
Q-12	**G-11**	**A-10**	**H-9**	**M-8**	**G-7**	**I-6**	**Q-5**	**R-4**	**P-3**
CAG	GGC	GCC	CAT	ATG	GGA	ATT	CAA	AGG	CCT
T-2	**S-1**	**T0**	**M1**	**K2**	**F3**	**M4**	**A5**	**E6**	**N7**
CAG	TCG	ACC	ATG	AAA	TTT	ATG	GCA	GAA	AAT
R8	**L9**	**T10**	**L11**	**T12**	**K13**	**G14**	**T15**	**A16**	**K17**
AGG	CTG	ACG	TTA	ACA	AAA	GGA	ACA	GCA	AAA
D18	**I19**	**I20**	**E21**	**R22**	**F23**	**Y24**	**T25**	**R26**	**H27**
GAT	ATT	ATA	GAA	CGA	TTT	TAG	ACG	AGA	CAT
G28	**I29**	**E30**	**T31**	**L32**	**E33**	**G34**	**F35**	**D36**	**G37**
GGG	ATT	GAA	ACA	TTA	GAA	GGC	TTT	GAT	GGC
M38	**F39**	**V40**	**T41**	**Q42**	**T43**	**L44**	**E45**	**Q46**	**E47**
ATG	TTT	GTT	ACA	CAA	ACT	TTA	GAA	CAA	GAA
D48	**F49**	**D50**	**E51**	**V52**	**K53**	**I54**	**L55**	**T56**	**V57**
GAT	TTT	GAT	GAA	GTG	AAA	ATT	TTA	ACA	GTT
W58	**K59**	**S60**	**K61**	**Q62**	**A63**	**F64**	**T65**	**D66**	**A67**
TGG	AAA	TCA	AAG	CAA	GCT	TTT	ACG	GAT	GCG
L68	**K69**	**S70**	**D71**	**V72**	**F73**	**K74**	**A75**	**A76**	**H77**
TTA	AAA	TCT	GAT	GTC	TTT	AAA	GCA	GCG	CAT
K78	**H79**	**V80**	**R81**	**S82**	**K83**	**N84**	**E85**	**D86**	**E87**
AAA	CAT	GTT	AGA	AGT	AAA	AAT	GAA	GAT	GAA
S88	**S89**	**P90**	**I91**	**I92**	**N93**	**N94**	**K95**	**V96**	**I97**
AGT	AGC	CCG	ATT	ATA	AAT	AAC	AAA	GTA	ATT
T98	**Y99**	**D100**	**I101**	**G102**	**Y103**	**S104**	**Y105**	**M106**	**K107**
ACA	TAT	GAT	ATA	GGC	TAT	AGT	TAC	ATG	AAA

Table S4. W67F IsdG Gene Sequence including N-terminal His_6-tag, short-linker, and TEV cleavage site. The polypeptide begins at S-1, after the S219V TEV cleavage.

M-22	**G-21**	**H-20**	**H-19**	**H-18**	**H-17**	**H-16**	**H-15**	**D-14**	**Y-13**
ATG	GGT	CAT	CAT	CAT	CAT	CAT	CAC	GAT	TAC
D-12	**I-11**	**P-10**	**T-9**	**T-8**	**E-7**	**N-6**	**L-5**	**Y-4**	**F-3**
GAT	ATC	CCA	ACG	ACC	GAA	AAC	CTG	TAT	TTT
Q-2	**S-1**	**T0**	**M1**	**K2**	**F3**	**M4**	**A5**	**E6**	**N7**
CAG	TCG	ACC	ATG	AAA	TTT	ATG	GCA	GAA	AAT
R8	**L9**	**T10**	**L11**	**T12**	**K13**	**G14**	**T15**	**A16**	**K17**
AGG	CTG	ACG	TTA	ACA	AAA	GGA	ACA	GCA	AAA
D18	**I19**	**I20**	**E21**	**R22**	**F23**	**Y24**	**T25**	**R26**	**H27**
GAT	ATT	ATA	GAA	CGA	TTT	TAG	ACG	AGA	CAT
G28	**I29**	**E30**	**T31**	**L32**	**E33**	**G34**	**F35**	**D36**	**G37**
GGG	ATT	GAA	ACA	TTA	GAA	GGC	TTT	GAT	GGC
M38	**F39**	**V40**	**T41**	**Q42**	**T43**	**L44**	**E45**	**Q46**	**E47**
ATG	TTT	GTT	ACA	CAA	ACT	TTA	GAA	CAA	GAA
D48	**F49**	**D50**	**E51**	**V52**	**K53**	**I54**	**L55**	**T56**	**V57**
GAT	TTT	GAT	GAA	GTG	AAA	ATT	TTA	ACA	GTT
W58	**K59**	**S60**	**K61**	**Q62**	**A63**	**F64**	**T65**	**D66**	**F67**
TGG	AAA	TCA	AAG	CAA	GCT	TTT	ACG	GAT	TTC
L68	**K69**	**S70**	**D71**	**V72**	**F73**	**K74**	**A75**	**A76**	**H77**
TTA	AAA	TCT	GAT	GTC	TTT	AAA	GCA	GCG	CAT
K78	**H79**	**V80**	**R81**	**S82**	**K83**	**N84**	**E85**	**D86**	**E87**
AAA	CAT	GTT	AGA	AGT	AAA	AAT	GAA	GAT	GAA
S88	**S89**	**P90**	**I91**	**I92**	**N93**	**N94**	**K95**	**V96**	**I97**
AGT	AGC	CCG	ATT	ATA	AAT	AAC	AAA	GTA	ATT
T98	**Y99**	**D100**	**I101**	**G102**	**Y103**	**S104**	**Y105**	**M106**	**K107**
ACA	TAT	GAT	ATA	GGC	TAT	AGT	TAC	ATG	AAA

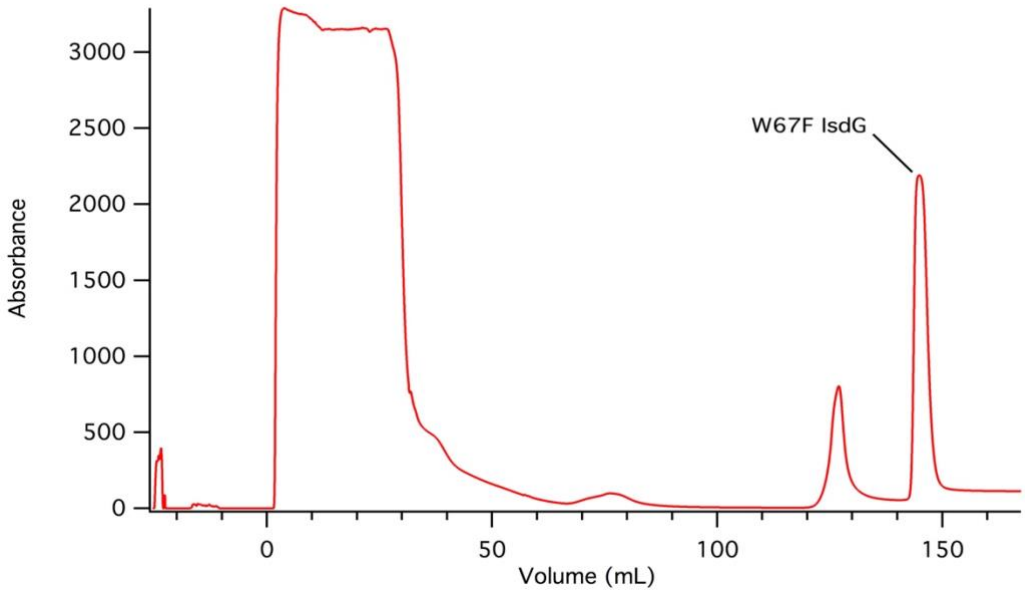

Figure S1. FPLC trace of W67F IsdG. The filtered lysate was loaded onto a nickel-charged HiTrap Chelating HP column (GE Healthcare) equilibrated with 50 mM Tris pH 7.4, 150 mM NaCl. The column was washed with a linear gradient of imidazole from 0 to 80 mM before W67F IsdG was eluted with 250 mM imidazole.

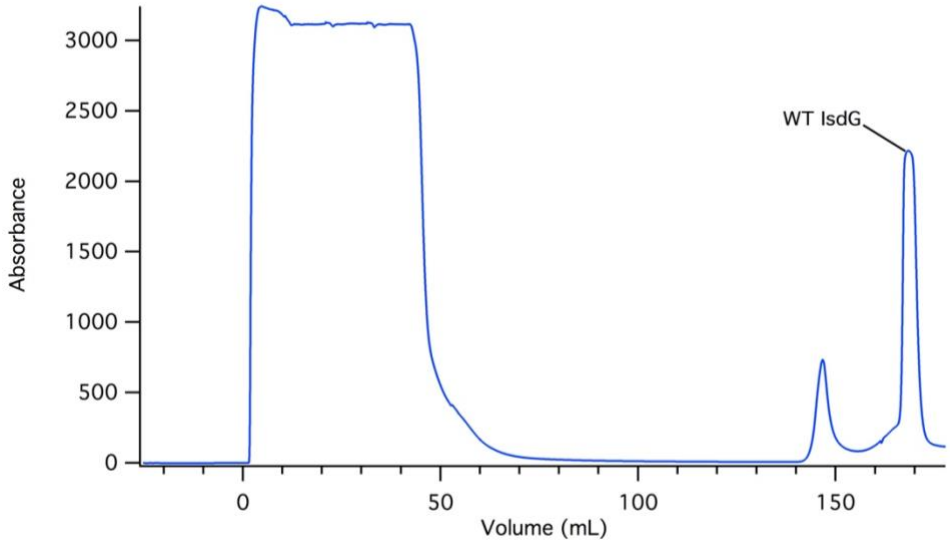

Figure S2. FPLC trace of WT IsdG. The filtered lysate was loaded onto a nickel-charged HiTrap Chelating HP column (GE Healthcare) equilibrated with 50 mM Tris pH 7.4, 150 mM NaCl. The column was washed with a linear gradient of imidazole from 0 to 80 mM before WT IsdG was eluted with 250 mM imidazole.